

**Neotectonic uplift and mountain building  
in the Alpine-Himalayan Belt**

*V.G. Trifonov, S.Yu. Sokolov and D.M. Bachmanov*

The book describes neotectonic uplifts producing mountain building in the Alpine-Himalayan Belt. This process began in the Oligocene as formation of local uplifts in zones of concentration of collision compression and accelerated in the Pliocene and Quaternary as the isostatic effect of decrease of density of the uppermost mantle and the lower crust by partial replacing of the lithospheric mantle by the asthenosphere material and retrograde metamorphism of high-metamorphosed rocks by asthenosphere fluids. These changes were initiated and kept up by the sub-lithosphere upper mantle flows that spread, according to the seismic tomography data, from the Ethiopian-Afar superplume and were enriched by fluids, reworking the transitional mantle layer beneath the future mountain belt. The upper mantle flows not only move lithosphere plates with all plate-tectonic consequences of this process, but also initiate transformations of the lithosphere that results in vertical movements producing mountain building. The book is intended for wide circle of geoscientists.

*Keywords:* Oligocene to Quaternary, neotectonics, uplift, mountain building, molasses, seismic tomography, lithosphere, asthenosphere, mantle flows

## Content

Introduction .....	5
Part 1. Neotectonic development of the central part of the Alpine-Himalayan Belt ..	9
1.1. Pre-history ( <i>V.G. Trifonov</i> ) .....	9
1.2. Neotectonic evolution of the Central Tien Shan ( <i>V.G. Trifonov, D.M. Bachmanov</i> ) .....	14
1.2.1. Changes in the regime of vertical movements during the neotectonic evolution .....	14
1.2.2. Horizontal shortening of the Earth's crust in the Oligocene-Quaternary ...	26
1.2.3. Contribution of compression to crustal thickening and uplift in the Central Tien Shan .....	31
1.2.4. The rise of the asthenosphere roof beneath the Central Tien Shan .....	33
1.2.5. Great thickness and density of the Central Tien Shan crust before its Cenozoic compression and possible transformation of the lower crust during the Quaternary uplift .....	34
1.2.6. Relative significance of different processes producing neotectonic uplift of the Central Tien Shan .....	35
1.3. Neotectonic evolution of the Pamirs and surrounding ( <i>V.G. Trifonov, T.P. Ivanova</i> ) .....	37
1.3.1. Mesozoic zoning and its deformation due to neotectonics .....	37
1.3.2. The Pamirs and Afghan-Tajik Basin .....	44
1.3.3. Recent geodynamics of the Pamir-Hindu Kush region .....	48
1.4. Neotectonic evolution of the Greater Caucasus ( <i>V.G. Trifonov</i> ) .....	53
1.5. Evolution of the Alpine-Himalayan Collision Belt in the Oligocene-Quaternary ( <i>V.G. Trifonov, T.P. Ivanova, D.M. Bachmanov</i> ) .....	57
1.5.1. Oligocene-Early Miocene (35-17 Ma) .....	57
1.5.2. Middle Miocene (16-11 Ma) .....	60
1.5.3. Late Miocene-Early Pliocene (10.0-3.6 Ma) .....	62
1.5.4. Late Pliocene-Quaternary (the last ~3.6 Ma) .....	63
1.5.5. Relationships between collision and tectonic uplift producing mountain building .....	72

1.5.5.1. Methodical Approach .....	72
1.5.5.2. Mountain building as a result of collision compression .....	73
1.5.5.3. Pliocene–Quaternary acceleration of tectonic uplift producing mountain building .....	76
1.5.6. Sources of neotectonic uplift in the Alpine-Himalayan Belt ( <i>V.G. Trifonov</i> ) .....	78
Part 2. Results of seismic tomography analysis of the mantle and deep sources of the Pliocene–Quaternary uplift .....	79
2.1. Seismic tomography profiling of the Alpine-Himalayan Belt ( <i>S.Yu. Sokolov</i> ) .....	79
2.2. A model of structural evolution of the mantle beneath the Tethys and Alpine-Himalayan Collision Belt in Mesozoic and Cenozoic and its geological consequences ( <i>V.G. Trifonov, S.Yu. Sokolov</i> ) .....	85
2.2.1. Ethiopian-Afar superplume and upper-mantle flows spreading away from it ( <i>V.G. Trifonov, S.Yu. Sokolov</i> ) .....	85
2.2.2. Cenozoic volcanism in the northern Arabian Plate and Arabian-Caucasus Segment of the Alpine-Himalayan Belt ( <i>V.G. Trifonov, D.M. Bachmanov, T.P. Ivanova</i> ) .....	93
2.2.2.1. Basaltic volcanism in the Arabian Plate .....	93
2.2.2.2. Correlation of the Cenozoic volcanism in the Arabian Plate and in the Arabian-Caucasus segment of the Alpine-Himalayan Belt .....	103
2.2.3. Intracontinental mantle seismic-focal zones in the Alpine-Himalayan Belt ( <i>V.G. Trifonov, T.P. Ivanova, D.M. Bachmanov</i> ) .....	107
2.2.3.1. The Pamir–Hindu Kush mantle seismic zone .....	107
2.2.3.2. The Vrancea mantle seismic megafocus .....	113
2.2.3.3. Origin of mantle seismicity .....	116
2.3. Plate tectonics and tectonics of mantle flows ( <i>V.G. Trifonov, S.Yu. Sokolov</i> ) .....	117
2.3.1. Development of plate tectonic theory .....	117
2.3.2. Tectonics of mantle flows .....	120
Conclusion .....	127
References .....	130

## Introduction

Obruchev (1948), introducing the terms *neotectonics* and *neotectonic* epoch, applied them to the process leading to the formation of the present-day topography that is distinguished by high-mountain systems, which did not exist earlier in the Mesozoic and Cenozoic geological history. In this book, we consider the tectonic movements, which gave rise to the contemporary topography of the central Alpine–Himalayan Orogenic Belt between the Carpathians and Balkan–Aegean region in the west and the Tien Shan, Kunlun, Tibet, and Himalayas in the east (Fig. 1)<sup>1</sup>.

In the first part of the book, we describe the history of neotectonic (Oligocene–Quaternary) movements that produced uplift of orogenic structures of the belt. Analyzing neotectonic evolution of the Central Tien Shan, Pamirs, Great Caucasus, and finally the orogenic belt as a whole, we show that their evolution includes two main stages. During the first long-time stage that lasted from Oligocene till the end of Miocene and even Pliocene in some regions, local uplifts formed. They were usually not higher than middle-level mountains (< 1500 m) and formed under collision compression as the results of isostatic compensation of thickening of the Earth’s crust in zones of concentrated deformation. During the second Pliocene–Quaternary stage, the height of the mountains increased 2–3 times. This intensification of tectonic uplift producing mountain building can not be explained by effects of the collision compression. It was caused by a decrease in the density of the crust and upper mantle under the effect of the asthenosphere, which was activated by fluids.

The second part of the book is devoted to deep-seated sources of the neotectonic processes mentioned above. The analyzing seismic tomography data demonstrate two important features of the mantle. First, in the eastern (Indonesian) part of the Alpine-Himalayan Belt, where subduction has continued till now, the higher-velocity subducted slabs became approximately horizontal at the depths of about 400–700 km and these sub-horizontal lenses spread beneath the adjacent continental upper mantle. The same continuations of the subducted slabs are known in the North-Western Pacific, where they were termed as stagnant slabs (Fukao et al., 2001), or big mantle wedges (BMW) (Zhao, 2009; Zhao et al., 2010). Second, in the more western mountain part of the Alpine-Himalayan Belt, sub-lithosphere low-velocity (hot and lower-dense) mantle flows were identified. They begin in the Ethiopian–Afar superplume rising from the lower mantle and spread beneath the orogenic belt.

<sup>1</sup> For the sake of brevity, these segments will be called further merely the Alpine–Himalayan Belt.

the Pamirs continued. In the east, it experienced pressure from the Tarim Block, the drift of which had a western component due to the left-lateral movements along the Altyn Tagh Fault with a rate that reached 1 cm/yr in the Quaternary. The Tajik–Karakum Block of the Turan Plate could move in the opposite direction because of the right-lateral displacement along the Main Kopet Dagh Fault (>2 mm/year in the Quaternary). The countermovement of flanks shortened the Pamirs in the W–E direction and stretched it in the N–S direction, so that the North Pamir Zone was thrust over the Afghan-Tajik Basin. The convergence of the Pamirs and Tien Shan was caused by this process, and the westward removal of sedimentary sequences from the area of maximal shortening has been occurring until now, as follows from geodetic and geologic evidence (Guseva et al., 1993; Trifonov et al., 2002).

Intensive Pliocene–Quaternary vertical movements, the magnitude of which during only the Quaternary exceeded 6 km, were the most important process at the late stage of neotectonic period. Uplifting was driven by ongoing stacking of crustal blocks and by decrease of density of the upper mantle and the lower crust. The deformation was most large-scale in the western Pamirs; therefore, its uplift rate in the Pliocene–Quaternary was higher than in the eastern Pamirs (Krestnikov et al., 1979). The Quaternary rise was accompanied by gravity-driven overthrusting at the northern, western and eastern flanks of the Pamirs and by extension in its axial zone (Lake Karakul Depression).

The decrease of density of the upper mantle in the Pamir–Kindu Kush–Karakorum region was justified by the seismological data on lowered seismic wave velocities to 0.1–0.2 km/s relative to their worldwide background (Vinnik, Lukk, 1974; Lukk, Vinnik, 1975; Vostrikov, 1994) and by analysis of the gravimetrical data (Artemjev, Kaban, 1994). The decrease of density could be a result of the partial replacement of the lithospheric mantle by the asthenosphere matter. In the process of collision deformation, big volumes of the former oceanic crust within the lithosphere were pressed into the mantle to depths of 40–70 km, where they underwent the high-pressure metamorphism, being partly transformed into garnet granulites and eclogites (see section 2.2.3.1). A part of them that had the lesser density than the surrounding mantle and did not subside because of this, could undergo the retrograde metamorphism with participation of the cooled asthenosphere fluids during uplift at the Pliocene–Quaternary stage of neotectonic deformation. This decreased the density of the lower crust rocks and produced additional uplift in the region.

## 1.4. Neotectonic evolution of the Greater Caucasus

To understand sources of uplift of the Greater Caucasus (GC), we estimated consequently the following characteristics: (1) thickness and composition of the Earth's crust before its deformation by compression; (2) values of transverse shortening, thickening and uplift of the crust because of the compression; (3) transformation of the deformed crust into the recent mountain system. The used data on the Mesozoic–Cenozoic geology of the GC are based on the publications (Milanovsky, Khain, 1963; Panov, 1988; Shcherba, 1993; Alpine history..., 2007; Marinin, Rastsvetaev, 2008). The main part of the GC formed in the margin of the post-Paleozoic Scythian Plate. Its part, weakly deformed in Mesozoic and Cenozoic is separated from the GC by the foredeeps, Azov-Kuban in the west and Terek-Derbent in the east (Fig. 15).

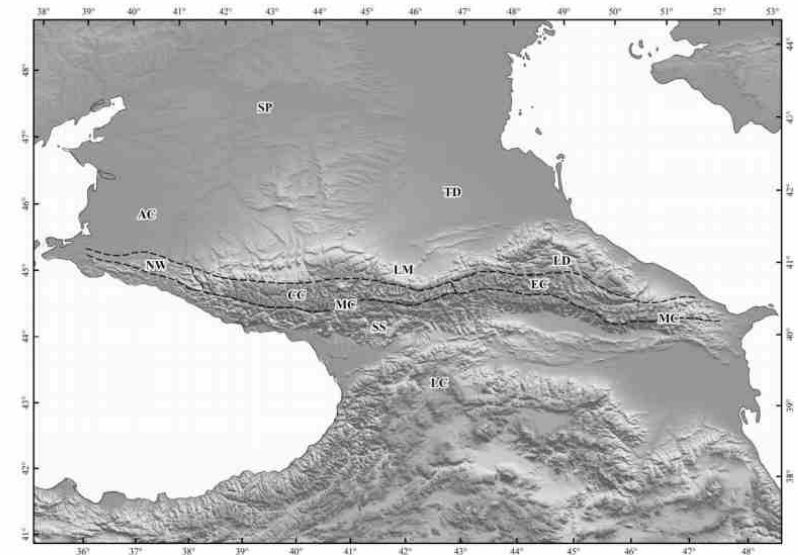


Fig. 15. The Greater Caucasus. AC, Azov-Kuban Basin; CC, Central Caucasus; EC, Eastern Caucasus; LC, Lesser Caucasus; LD, Limestone Daghestan; LM, Laba-Malka Zone; MC, Main Caucasus Fault; NW, North-western Caucasus; SP, Scythian Platform; SS, Southern Slope Zone; TD, Terek-Derbent Basin

The transitional Laba-Malka Zone (LMZ), including the East Balkar subzone and Limestone Daghestan, extends along the northern slope of the GC (Alpine history..., 2007). The thickness of the LMZ sedimentary cover varies from 5–5.5 km in the central part to 6.5–7 km in the east and ~10 km in the north-west. The GC itself consists of the northwestern, central and eastern segments. The North-Western

Caucasus is composed of the Jurassic, Cretaceous, and Paleogene (in the peripheral parts) deposits; their total thickness is up to 14 km. The same deposits were ~11 km thick in the Eastern Caucasus in the Early Miocene, although that region was subjected to the Cimmerian (pre-Bathonian and pre-Callovian) folding. In the Central Caucasus, the Lower and Middle Jurassic deposits were intensively deformed by the Cimmerian folding and preserved only in compressed synclines between the Paleozoic blocks. The Upper Jurassic to Paleogene deposits covered this uplift of the basement. We estimated their total thickness in the Early Miocene as ~2–2.5 km. The southern part of the GC (Zone of Southern Slope, ZSS) is separated from the GC itself by the Main Caucasus Reverse Fault. Near this fault, the ZSS is composed of the Lower and Middle Jurassic deposits, which are overlaid with the Upper Jurassic to Paleogene mainly flysch deposits farther to the south. Both parts of the ZSS represented a single basin with the 15–20-km total thickness of the sediments in the Early Miocene. Reconstructing the Earth's crust structure of different zones of the GC in the Early Miocene (Table 3), we considered that the crust was in isostatic balance at that time and the land surface differed from the sea level not more than to ~300 m. We estimated the average density of the sedimentary cover as 2.5 g/cm<sup>3</sup> and considered that the density of the basement beneath thick sedimentary basins increased up to 2.9–2.93 g/cm<sup>3</sup>, by analogy with other similar structures (Artyushkov, 1993).

Tectonic zone	Thickness of J–Pg cover	Thickness of basement	Density of basement	Thickness of the crust
Zone of the Southern Slope	18±2 km	~16±1 km	2.93 g/cm <sup>3</sup>	~34±2 km
North-Western Caucasus	~14 km	~21 km	2.9 g/cm <sup>3</sup>	~35 km
Central Caucasus	2–2.5 km?	~40 km	2.83 g/cm <sup>3</sup>	~42 km
Eastern Caucasus	~11 km	~25 km	2.87 g/cm <sup>3</sup>	~36 km
LMZ, western segment	~10 km	~26 km	2.85 g/cm <sup>3</sup>	~36 km
LMZ, central segment	~5 km	~34 km	2.84 g/cm <sup>3</sup>	~39 km
LMZ, eastern segment	~7 km	~31 km	2.85 g/cm <sup>3</sup>	~38 km

Table 3. Calculated characteristics of the Earth's crust of Greater Caucasus in the Early Miocene. LMZ is the Laba-Malka Zone

The Mesozoic and Cenozoic deposits of the GC are deformed by folds and faults. We analyzed deformation that was due to compression and resulted in transverse shortening of the Earth's crust. Using the published data (Gamkrelidze P.D., Gamkrelidze I.P., 1977; Panov, 2002; Alpine history..., 2007; Yakovlev, 2006, 2008,

2012; Marinin, Rastsvetaev, 2008), supplemented by our calculation of shortening in the LMZ and Limestone Daghestan, we estimated the transverse shortening and, correspondingly, the deformational uplift of the land surface in different zones by equations (1) and (2) in section 1.2.3 (Table 4).

Tectonic zone	Initial thickness of the crust, km	Shortening	Post-folding thickness of the crust, km	Thickening of the crust, km	Isostatic uplift, km
ZSS	~34±2	~50%	~68±4	~34±2	~4.8–5.4
North-western Caucasus	~35	~20%	~44	~9	~1.4
Central Caucasus, Cimmerian	~38?	20–30%?	~48–52?	~10–14?	~1.5–2.1?
Central Caucasus, Late-Alpine	~42	10–20%?	~47–52	~5–10?	~0.8–1.5?
Eastern Caucasus, Cimmerian	~38	20–30%	~48–52	~10–14	~1.5–2.1
Eastern Caucasus, Late-Alpine	~36	10–20%	~40–45	~4–9	~0.6–1.4
Limestone Daghestan	~38	10–20%	~42–48	~4–10	~0.6–1.5
LMZ, east and center	~36–39	<10%	~39–43	<3–4	<0.4–0.6

Table 4. Calculated values of the fold thickening of the Earth's crust and related isostatic uplift of the land surface in the Greater Caucasus

The age of main phase of the late Alpine deformation is under discussion. We consider it to be post-Maykopian, i.e., late Early and Middle Miocene, because the Maikopian (Oligocene – Lower Miocene) marine deposits covered the Greater Caucasus and the Maikopian Basin inherited the previous sedimentation in the region (Kopp, Shcherba, 1993; Shcherba, 1993). But the actual situation is more complicated. In the Central Caucasus, the significant deformation occurred at the pre-Bathonian and pre-Callovian time. As a result, the area became the uplifted block of the consolidated crust. Thickening and isostatic uplift of the Central Caucasus crust explain erosion of the Lower and Middle Jurassic deposits and exhumation of the Paleozoic basement. However, the Cimmerian deformation in the Eastern Caucasus did not produce significant pre-Late Jurassic uplift and erosion. The *Moho* is characterized there by the boundary velocities  $V_p=8.2–8.3$  km/s. The seismic profiling found the layer with the velocities decreased up to 7.8 km/s under the *Moho* at the depths of 59–66 km and the discontinuity with boundary velocity  $V_p=8.5$  km/s under it (Krasnopevtseva, 1984). Perhaps, this lower discontinuity is a relic of the former bottom of the crust. Its lower layers were subjected to metamorphism and

their density came nearer to the mantle one. The densification compensated the thickening of the crust in the Eastern Caucasus and the Cimmerian uplift was not significant. The calculated crust thickness after the late Alpine deformation differ in majority of the GC zones from the recent thickness of the Earth's crust, as it is determined by seismic profiling (Krasnopevtseva, 1984; Grekov et al., 2008). The ZSS demonstrates the highest difference. This abnormally high calculated crust thickness and uplift are not corroborated by geophysical, geomorphological and geological (composition of molasses) data. Perhaps, there, as in the Eastern Caucasus at the Cimmerian epoch, the densification of the lower crust compensated the deformational thickening of the crust.

During the main phase of the late Alpine deformation and immediately after it, i.e., in the Middle and early Late Miocene, the fine-grained material dominated in the molasses. Probably, the magnitudes of deformational uplands did not exceed mid-level mountains (up to ~1.5 km). This corresponds to calculated elevation, except the ZSS (Table 4). Essential portions of the pebbles arrived in molasses of the GC and its surrounding only at the end of Miocene and became abundant at the Pliocene (Milanovsky, Khain, 1963; Shcherba, 1993). Designing the conditional pre-orogenic surface of planation, Milanovsky (1968) estimated the magnitudes of Late Cenozoic rise in different zones of the GC (Table 5).

Zone	$h_0$ , km	$S_0$ , km	$h_F$ , km	$S_F$ , km	$H_F$ , km	$h_R$ , km	$S_R$ , km	$H_R$ , km
ZSS	32–36	16–20	64–72	32–40	4.8–5.4	35 (W) – 45–50 (C– E)		≤1.5 (W) – up to 2.5– 3.5 (C–E)
NW Caucasus	~35	~14	~44	~17	~1.4	~41		1–1.5
Central Caucasus	~42	~2.5 (0– 10)	~47–52		~0.8–1.5?	50–55	~2	2.5–3.5
Eastern Caucasus	~36	~11	~40–45	~13	~0.6–1.4	54–55	~10	≥3
LMZ	36–39	5–10	~39–43	~6–11	<0.4–0.6	~43		0.5–2
LD	~38	~7	~42–48		~0.6–1.5	~45		1–2

Table 5. Correlation between the calculated values of the Earth's crust thickness before and after the main phase of the Late-Alpine folding and post-folding uplift and the recent values of the crust thickness and uplift of the land surface.

$h_0$  is the initial (before the Late-Alpine folding) thickness of the crust;  $S_0$  is the initial thickness of the sedimentary cover;  $h_F$  is the post-folding thickness of the Earth's crust;  $S_F$  is the post-folding thickness of the sedimentary cover;  $H_F$  is the post-folding uplift of the land surface;  $h_R$  is the recent position of the *Moho* surface (below s.l.);  $S_R$  is the recent thickness of the sedimentary cover;  $H_R$  is the recent uplift of the land surface (above s.l.); LD, Limestone Daghestan.

Everywhere, except the North-Western Caucasus and ZSS, the recent altitudes are higher than the calculated deformational uplift. This means that the GC grew more intensively from the end of Miocene (Milanovsky, 1968) or the beginning of Pliocene (Map of neotectonics of the south ..., 1971) than it was caused by the deformational thickening of the crust. The magnitudes of additional uplift reached 1.5–2 km in the Central and Eastern Caucasus. The additional uplift probably occurred also in the zones, where the difference between  $H_F$  and  $H_R$  is unessential. For example, the topographic reversal presupposes erosion of the deformational topography and, correspondingly, additional uplift in the North-Western Caucasus.

## 1.5. Evolution of the Alpine-Himalayan Collisional Belt in the Oligocene-Quaternary

Two main stages of deformation, metamorphism and tectonic uplift, the Oligocene–Miocene (or Oligocene–Early Pliocene) and the Pliocene–Quaternary ones, are distinguished in the Alpine-Himalayan Belt. The stage 1 is differentiated into three substages differing in direction of compression of the orogenic belt related to the motion of the Gondwana plates (Trifonov, 1999; Ivanova, Trifonov, 2005; Rukieh et al., 2005). These substages correspond to Oligocene–Early Miocene, Middle Miocene, and Late Miocene–Early Pliocene.

### 1.5.1. Oligocene–Early Miocene (35–17 Ma)

Compressive deformation, which started in the east of the region at the end of the Middle Eocene continued in the Oligocene and resulted in closure of the sub-oceanic Sabzevar Trough (Kazmin et al., 2010) and the Indus–Zangpo Zone (Aitchison et al., 2007) (Fig. 16). The intense compressive deformations, which took place in the Herat Zone in northern Afghanistan and in the northwestern Pamir–Hindu Kush brought about squeezing of the South-Western Pamir to the east and its thrusting over the zone of the South-Eastern Pamir (Ivanova, Trifonov, 2005; see section 1.3.1). Transverse compression in the northern part of the Quetta Zone was expressed in folding of the Eocene Katawaz Trough and formation of the NE-trending thrust faults in the Khost, Tarnaka, and Khash Rud ophiolite zones (Geology and Mineral Resources..., 1980; Tapponnier et al., 1981).

Syn- and postfolding uplifts arose in the compressed zones. The Oligocene–Miocene conglomerates overlapped the deformed rocks of the Indus–Zangpo Zone

with unconformity (Tewari, 1964; Aitchison et al., 2007) and were found in the foothills of the Pamir (Shvolman, 1977) and Kunlun (Recent geodynamics..., 2005). Differential vertical movements spread over the Tien Shan. In the Central Tien Shan, the Oligocene fine-pebble conglomerate and more fine clastic sediments are known (Shultz, 1948; Makarov, 1977; Dmitrieva, Nesmeyanov, 1982; Chediya, 1986). Local clastic material occurs and occasionally dominates in the pebbles (Bachmanov et al., 2009). This implies that the recent ridges as provenances of clastic material and the basins as depocenters originated in the Oligocene. In the Early Miocene, vertical movements became more sluggish; deluvial and lacustrine clayey sediments locally with evaporites were deposited at that time.

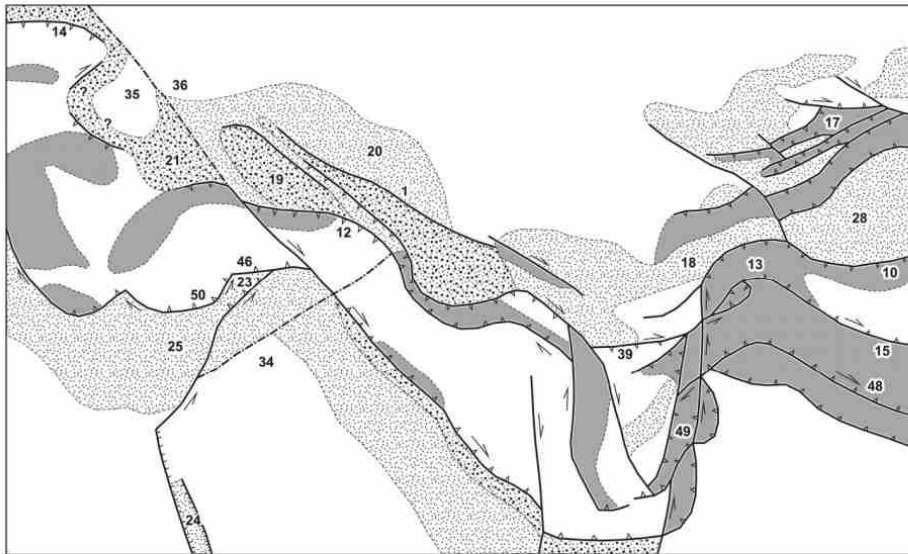


Fig. 16. Conceptual map of tectonic elements of the Alpine-Himalayan Belt at the end of the Oligocene (~25 Ma ago); modified after (Bachmanov et al., 2009; Bazhenov, Burtman, 1990; Dronov, 1980; Golonka, 2004; Alpine history..., 2007; Ivanova, Trifonov, 2005; Kazmin et al., 2010; Kopp, Shcherba, 1993; Robertson et al., 2004; Rukieh et al., 2005; Trifonov et al., 2012; Trifonov, Sokolov, 2014). See fig. 1 for legend

Judging from the relatively fine clastic material and shallow (a few hundreds of meters) incision of valleys formed at that time (Makarov, 1977; Chediya, 1986), the vertical range of the Oligocene topography in the Central Tien Shan did not exceed a kilometer. The anomalously coarse conglomerates of the Minkush–Kökömeren ramp are a product of destruction of reactivated Late Paleozoic nappes and unrelated to significant hypsometric contrast (Bachmanov et al., 2008). The fine clastic molasses

in the foothills of the Pamir and Hindu Kush (Afghan–Tajik Basin) and Kunlun (south of the Tarim Basin) indicate that no high mountains existed at that time. Nevertheless, the isotopic data on the paleosol in Central Tibet show that high mountains existed there ~26 Ma ago (De Celles et al., 2007). A high isostatic uplift at that time is also suggested in the South-Western Pamir, the upper crustal sheet of which, reaching 25 km in thickness, is thrust over the continental crust of the South-Eastern Pamir (The Earth’s crust and upper mantle..., 1981; see also section 1.3.1). These high mountains were not widespread and were later subjected to erosion.

In the Arabian–Caucasus segment of the orogenic belt, the subduction in front of the South Taurus led to the formation of the accretionary wedge on the northern slope of the Kilikia–Adana Trough in Late Eocene–Early Oligocene. This wedge is composed of fragments of the Mesozoic oceanic crust and its Lower Paleogene cover. The blocks of carbonate cover of the Taurides slid over them. The process completed with the collision of the Taurides with the Arabian Plate in the northeast of this region and overlapping of the accretionary wedge by Lower Miocene sediments (Robertson, 2000; Robertson et al., 2004). A relic of the southern margin of this basin was retained in the southwest. In the Early Miocene (~17 Ma ago), it was isolated by the renewed Cyprus arc, and the Levantine Basin at the southern margin of Tethys began to subduct beneath this arc. Deformation reached a culmination at that time. The sharp angular unconformity between the Eocene and Helvetian is documented in the northwest of Syria (Rukieh et al., 2005).

Deformation developed in other zones of the Arabian–Caucasus Orogenic Belt up to the southern flank of the Caucasus part of the Carpathian–Caucasus system of troughs. Their underthrusting beneath the Lesser Caucasus was accompanied by formation of flysch along with tectonic and gravity mixtures (Leonov M.G., 1975; Shcherba, 1994; Alpine history..., 2007). The troughs themselves did not undergo deformation. In the Oligocene, they even locally deepened despite a global regression, especially intense in the early Late Oligocene (Vail, Mitchum, 1980), whereas an epicontinental sea spread over the entire Greater Caucasus and the adjacent Scythian Plate adjacent to the Caucasus and the Carpathians (Kopp, Shcherba, 1993). The supply of clastic material into the sedimentary basin was reduced in the Early Miocene.

The origination of a graben on the spot of the future Aden–Red Sea Rift was the most important event in the Oligocene, which initiated moving of Arabia apart from the African Plate. In this connection, the Dead Sea Transform arose in the Early Miocene (~20 Ma ago) (Garfunkel, Ben-Avraham, 2001). Its northern segment

extended along the continental slope of the Levantine Basin (Rukieh et al., 2005), inheriting an earlier transform zone.

In the Balkan Mountains, the Late Eocene phase of thrusting was followed by development of a foredeep, where flysch sedimentation gave way to deposition of molasses (Golonka, 2004). The displacement of the Carpathian inner zones gave birth to the Carpathian arc, which completed by thrusting of the detached nappes of the Northern Carpathians over the foredeep at the end of the Early Miocene.

The Oligocene uplifts (mainly low-mountain as judged from the composition of the piedmont molasses) were confined to compression zones in the west of the belt. Except for the Caucasus troughs of the Paratethys, the uplifts grew in area, while the sediments in the epicontinental basins, e.g., in northern Arabia, were related to the regressive phase of the Paleogene sedimentation cycle. This was probably caused by increase in collisional compression, though it can be partially explained by the global drop of ocean level.

All structural units of the orogenic belt, which underwent compressive deformation in the Oligocene and Early Miocene extend W–E or in north-eastern directions. This implies that the principal compression axis was oriented in the north-northwestern direction, which coincides with the directions of movement of the Gondwanan plates.

### 1.5.2. Middle Miocene (16–11 Ma)

During the second substage (end of the Early Miocene and the Middle Miocene), the most intensive lateral displacement and deformation of crustal blocks took place in the east of the belt corresponding to the region of the Indian–Eurasian collision. The Himalayas, Karakoram, and NW-trending Pamir zones were involved in deformation and thrusting accompanied by a peak of metamorphism and granite formation (Searle, 1991, 1996; Ivanova, Trifonov, 2005) (Fig. 17). At the same time, the intensity of tectonic movements decreased in the Central Tien Shan, where Oligocene uplifts extended in the ENE direction. The average rate of erosion became lower than in the Oligocene (Chediya, 1986). The Miocene lacustrine fine clastic sand-shale sediments are predominant, whereas alluvial sediments are second in abundance (see section 1.2.1). The areas of sedimentation expanded having overlapped some Oligocene uplifts (Bachmanov et al., 2009). Each sedimentary basin was a chain of lakes connected by permanent or intermittent channels. The basins were separated by flat uplifts, which act as additional provenances. To the south and the east, approaching the present-day Kakshaal-Too Range and the Khan Tengri

Massif, the clastic material becomes coarser, indicating higher elevations and more intensive erosion. They were the main sources of removed clastic material. Carbonate interlayers were replaced with evaporites moving away from the uplifts.

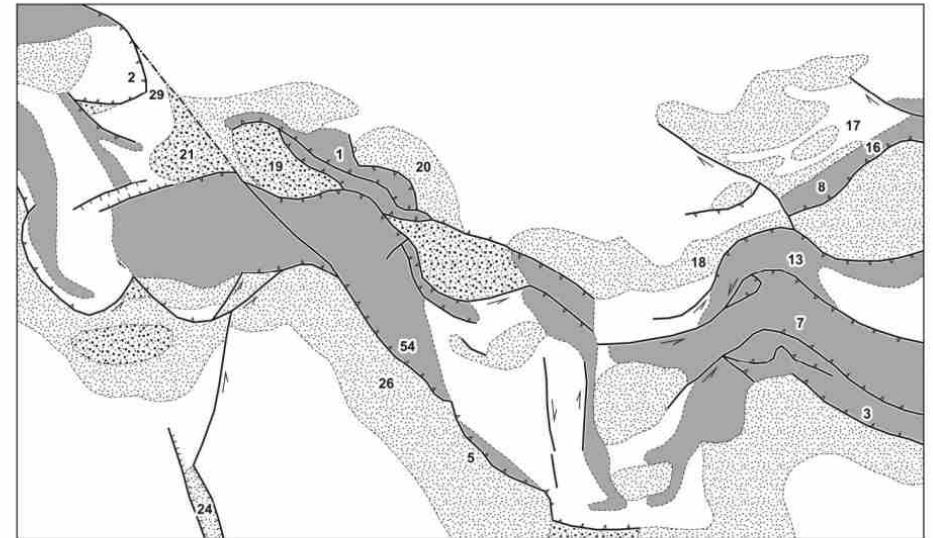


Fig. 17. Conceptual map of tectonic elements of the Alpine-Himalayan Belt at the Middle Miocene (~18 Ma ago); modified after (Artyushkov et al., 1996; Bachmanov et al., 2009; Golonka, 2004; Alpine history..., 2007; Ivanova, Trifonov, 2005; Kazmin et al., 2010; Kopp, Shcherba, 1993; Rukieh et al., 2005; Searle, 1991, 1996; Tapponier et al., 1981; Trifonov et al., 2012; Trifonov, Sokolov, 2014). See fig. 1 for legend.

Evidence for rearrangement of the principal compression direction with its shift to the northeast in the late Early and Middle Miocene was also documented in the western segments of the belt. A tectonic quiescence in the northwest of the Arabian Plate came with development of the Helvetian–Tortonian sedimentation cycle. The intensive movements along the Main Thrust of Zagros led to the closure of the Neotethys relic basin between the Arabian Plate and the Sanandaj–Sirjan Zone (Golonka, 2004). This event initiated onset of the development of the Mesopotamian Foredeep, which inherited the formerly sagging northeastern part of the plate. Folding started to develop at the northeastern flank of the trough in the late Middle–early Late Miocene.

The Caucasus troughs of the Paratethys were shoaled and then closed; at the end of the second stage, their sedimentary fill underwent folding (Kopp, Shcherba, 1993; Alpine history..., 2007). Thrusting of the Outer zone of the Eastern Carpathians over the Focsani Basin of the Carpathian Foredeep in the late Middle–early Late Miocene

was probably also related to the rearrangement of compressive stresses (Artyushkov et al., 1996). The thickness of the sedimentary cover in the Eastern Carpathians is now estimated at 8–12 km and initially could have been 10–14 km. Such an increase in the thickness of the sedimentary cover did not bring about a rise of the surface to the calculated value of 1.5–2.4 km, and the surface remained at a height of ~0.5 km. Thus, the uplift to 1–2 km was compensated by compaction of matter at a deeper level of the lithosphere. A similar phenomenon probably took place at the southern slope of the Greater Caucasus, where intensive folding and stacking of sedimentary sequences also did not lead to the formation of high mountains. Judging from the composition of the clastic complexes, highlands were not formed in other regions of the belt either. Moreover, the Pannonian Basin was formed on the place of the deformed inner zones of the Carpathians.

### 1.5.3. Late Miocene–Early Pliocene (10.0–3.6 Ma)

During the third, Late Miocene–Early Pliocene substage, the prevalent orientation of compression again became north-northwestern or nearly N-trending. The peak of diastrophism fell on the Messinian. A system of south-vergent thrusts developed on the southern slope of the Greater Caucasus (Fig. 18). At the southern flank of the region of interaction of the Arabian and Eurasian plates, the main phase of folding and thrusting took place in the Palmyrides. Folding in the Hellenides and thrusting in the Pamir were resumed. The fold–thrust zones expressed in the topography shifted to the south from the Main Thrust of Zagros and the Taurus (Bitlis) Thrust. In the Himalayas, such a propagation was marked by shift of the maximum displacements and deformation to the zone of the Frontal Fault.

In some intermontane basins of the Central Tien Shan, the Upper Miocene sequences were enriched in coarse clastic rocks, which gave way to fine clastic rocks upsection, in the Lower Pliocene. These coarse clastic rocks were products of destruction of the Late Paleozoic tectonic nappes; i.e., of activation of horizontal rather than vertical movements (Bachmanov et al., 2009). In some places, for example, in the Greater Caucasus (Kopp, Shcherba, 1993), the Late Miocene displacements and folding resulted in formation of dissected topography; however, the composition of clastic material in the intermontane basins and foredeeps indicates that the uplifts were characterized here, as in other segments of the belt, by moderate height of mountains.



Fig. 18. Conceptual map of tectonic elements of the Alpine-Himalayan Belt at the Messinian (~6 Ma ago); modified after (Artyushkov et al., 1996; Bachmanov et al., 2009; Golonka, 2004; Alpine history..., 2007; Ivanova, Trifonov, 2005; Kazmin et al., 2010; Kopp, Shcherba, 1993; Rukieh et al., 2005; Searle, 1996; Tappinier et al., 1981; Trifonov et al., 2012; Trifonov, Sokolov, 2014). See fig. 1 for legend

### 1.5.4. Late Pliocene–Quaternary (the last ~3.6 Ma)

The contemporary network of large active faults of the belt was formed by the Late Pliocene. The displacements along these faults (mainly strike-slip) indicate approximately N-trending orientation of the principal compression axis. In the northwest of Arabia, the onset of the fourth stage (4.0–3.5 Ma) was accompanied by rearrangement of the northern segment of the Dead Sea Transform. While in the Miocene, its main branch extended along the continental slope, now the main displacements concentrate along the Yammunneh and El Gharb segments (Rukieh et al., 2005) (Fig. 1). Approximately at the same time, the East Anatolian and North Anatolian Fault Zone, as well as the Main Recent Fault of Zagros demarcating the present-day plate boundaries (Saroglu, 1988; Trifonov, 1999; Westaway, 2004; Westaway et al., 2006), eventually formed.

The rates of vertical tectonic movements sharply increased over the last 5–2 Ma. The height of mountains at least doubled or tripled. The contemporary mountain systems and high plateaus were formed during this time, when coarse molasses were deposited in the foredeeps and intermontane basins. The most significant increase in uplifting is established in Central Asia (Fig. 19). The onset of acceleration of vertical

movements was not synchronous. The average height of the Himalayas has increased by over 3 km (Mörner, 1991) and the Central Tien Shan by ~2 km (Krestnikov et al., 1979; Chediya, 1986; Trifonov et al., 2008) since the Early Pleistocene (~2 Ma). The rapid rise of Tibet started 2.8–2.4 Ma ago and reached 2500–3600 m; the Kunlun and Tarim have grown simultaneously for 2600–3100 and ~1200 m, respectively (Mörner, 1991; Li Jijun, 1995; Recent geodynamics..., 2005). This yields an average rate of growth of Tibet and the Kunlun as 1.0–1.5 and 1.0–1.2 mm/yr, respectively. The particular substages of rapid uplift are outlined; thus, the rate of uplifting increased with time. The last substage began at the end of the Middle Pleistocene and the velocity of uplifting during this substage locally reached 10 mm/yr. According to the data of recurrent leveling, the velocity of contemporary uplift of Tibet is 6.8 mm/yr, on average, and increases from the Kunlun and northeastern Tibet to the Himalayas (Zhang Qingsong, 1991). Over the last 5 Ma, the Pamirs has grown ~2 km on average.

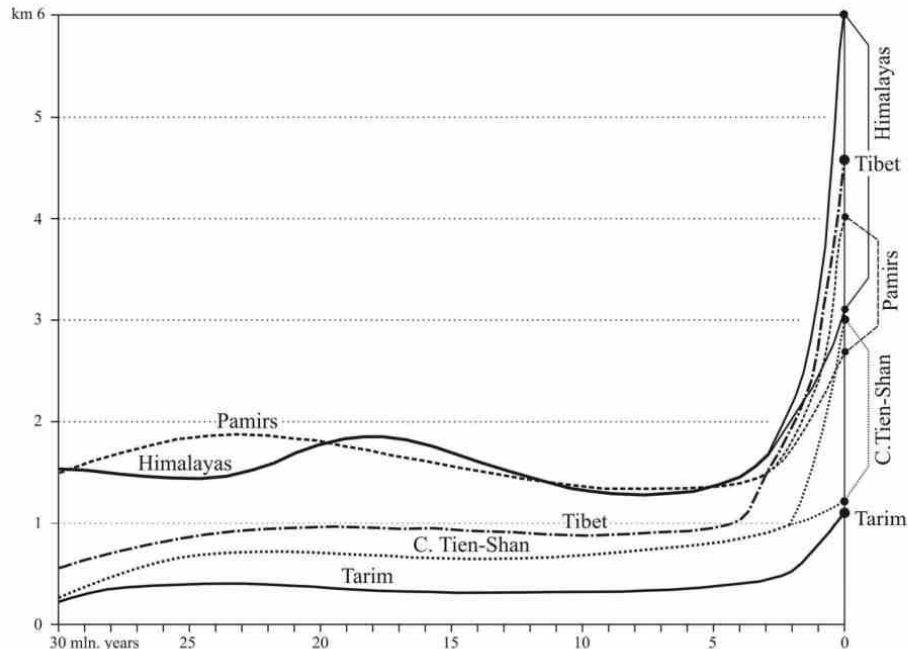


Fig. 19. Acceleration of mountain rise in High Asia in the Pliocene-Quaternary, modified after (Trifonov et al., 2012). At the right, the lower calculated curves showing what heights would be reached by the Pliocene-Quaternary uplift only as a result of increased compression, are compared with the upper curves showing the actual heights of the Himalayas, Pamirs, and Central Tien Shan

The intense mountain growth in the Pliocene and Quaternary has been established in the Greater Caucasus (Milanovsky, 1968; see also section 1.4), the Carpathians (Artyushkov et al., 1996), the Alps (Artyushkov, 1993), and other mountains of Southern Europe (Ollier, 2006). To estimate the Quaternary uplift in the Lesser Caucasus, we studied stratigraphy and tectonics of the Upper Pliocene–Quaternary deposits in NW Armenia (Trifonov et al., 2014, 2015). This territory is formed by the southern Javakheti volcanic ridge and adjacent basins, the Upper Akhurian in the west and the Lori in the east (Fig. 20). The Bazum Ridge with the Mesotethys suture borders the area to the south. Basalts, basaltic andesites, and dacites that cover the Pliocene volcanic formation and compose the southern Javakheti Ridge and bottoms of the adjacent basins are dated by the K-Ar technique in the time interval between ~2.5 and ~1.85 Ma. In the basins, these volcanic rocks underlie tuffaceous-clastic deposits. We divided them to the Karakhach and Kurtan units. By a combination of paleomagnetic, SIMS  $^{238}\text{U}$ - $^{206}\text{Pb}$ ,  $^{40}\text{Ar}/^{39}\text{Ar}$ , K-Ar and paleontological including pollen methods, the lower Karakhach unit was dated at 1.85–1.75 Ma and the age of the upper Kurtan unit was estimated as the Upper Calabrian (including the Jaramillo subchron) and the lowest Middle Pleistocene, i.e. ~1.2–0.5 Ma. The episodes of eruptions of andesites (~1.7 Ma) and dacite pumices and ashes (1.4 – 1.5 Ma) occurred between accumulation of these two units.

For estimation of magnitudes of the following rise of the area, it is important that the Kurtan unit covers volcanic rocks as a vast mantle. This means that topography was relatively flat. After accumulation of the Kurtan unit, the area was undergone to flexure-fault deformation and was uplifted. We can estimate the magnitude of uplift by intensity of incision of recent channels to the volcanic surface covered by the Kurtan unit. The incision reaches 370 m in the most upstream Debed River. Excluding the 20-meter effect of the Baku transgression of the Caspian Sea that was a final basis of erosion for the drainage system of the area, we conclude that the incision, approximately corresponding to the magnitude of uplift of the eastern Lori Basin, reached 350 m (Fig. 21). The rise reached as minimum 500 m in the Upper Akhurian Basin. The Karakhach Pass and, correspondingly, the Javakheti Ridge that is the northern continuation of the pass rose to ~500 m relative to the Lori Basin. The flexural bend of the basalts in the southern side of the Lori Basin expresses the minimum several hundred meters uplift of the Bazum Ridge relative to the basin. These values correspond to the average rates of uplift at 0.7–1 mm/yr for the basins and 1.2–1.6 mm/yr for the ridges during the last ~0.5 Myrs.

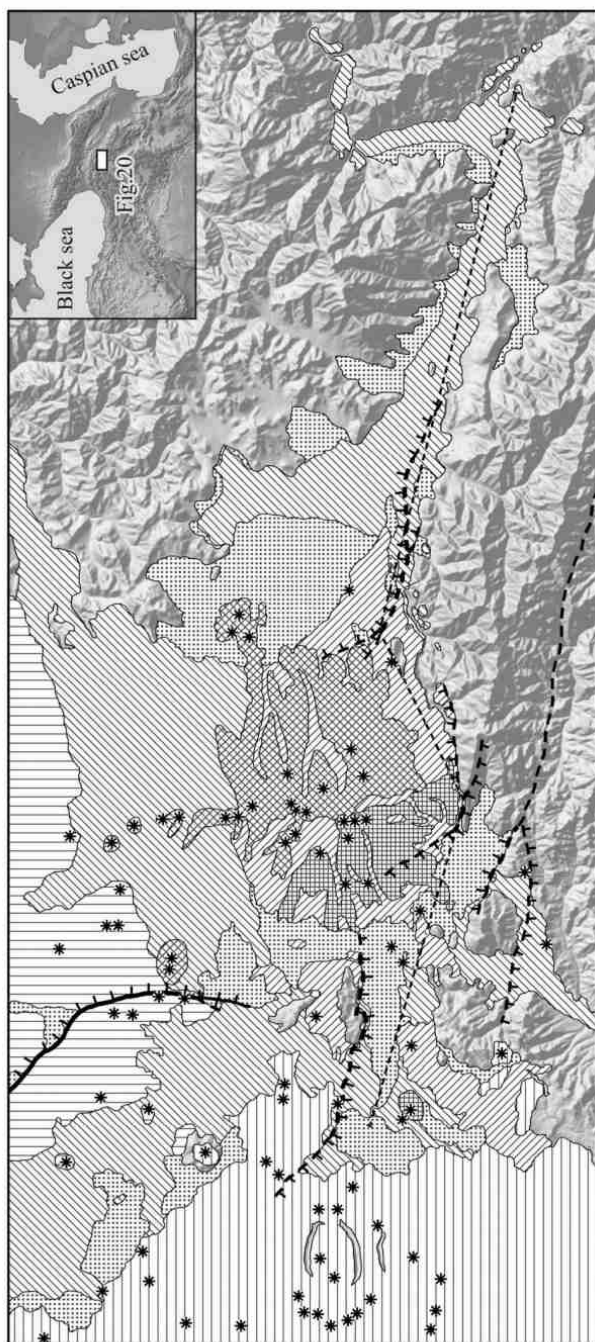


Fig. 20. Upper Pliocene and Pleistocene volcanic units in the southern Javakheti Ridge, Upper Akhurian and Lori basins; the dotted line shows position of the Fig. 21 profile; compiled by V.A. Lebedev with additions and corrections of V.G. Trifonov and D.M. Bachmanov.

1, unit I, Pliocene (mainly Upper Pliocene), basalts, andesites and more acid rocks including obsidians; 2, Upper Pliocene, basalts and andesites that are present in the Georgian part of the region and corresponds to the third phase of the Georgian volcanism, 2.7–2.4 Ma (Lebedev et al., 2008); 3, unit II, Gelasian basalts and basaltic trachyandesites; 4, unit III, upper Gelasian basaltic trachyandesites, trachyandesites and andesites; 5, unit IV, upper Gelasian dacites; 6, unit V, lower Calabrian basaltic trachyandesites, trachyandesites and andesites; 7, Quaternary sediments; 8, Middle-Late Quaternary flexure-fault zones; 9, volcanoes and extrusive domes. Geological sections: Ag, Agvorik; Ar, Ardenis; Dm, Dmamisi; Ka, Karakhach; Ko, Koghnes; Kr, Krasar; Kuf, Kurtan I; Kulfi, Kurtan III; Mu, Muradovo; Va, Vardaghybur; Ya, Yaghdan. 1–10, sites of K-Ar sampling. 12–15, other sites of observation

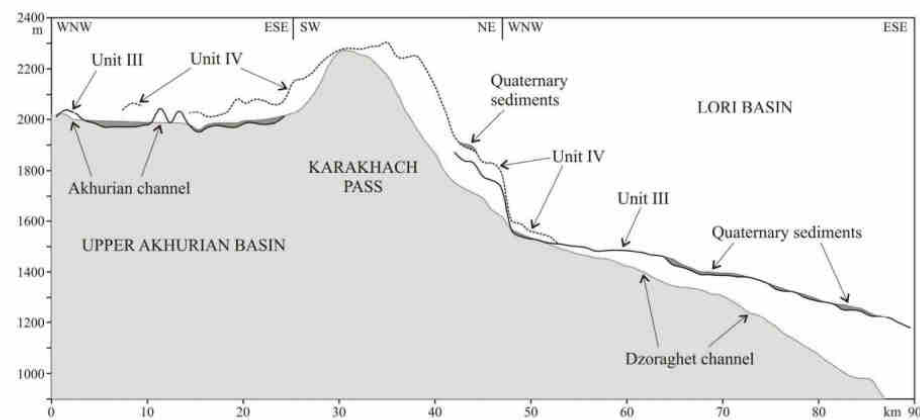


Fig. 21. W–E-trending geological-geomorphological profile along the Upper Akhurian Basin, Karakhach Pass and southern Lori Basin; compiled by D.M. Bachmanov and V.G. Trifonov

At the northwestern end of the Mesopotamian Trough (middle reaches of the Euphrates River), the lagoon and lacustrine sedimentation continued into the Early Pliocene, but then it gave way to coarse clastic alluvium fed by anticline uplifts propagating to the south. At the Syrian shore of the Mediterranean Sea (Fig. 22), a rapid growth of the Coastal Anticline has been established. The anticline began to evolve in the Miocene, when its axial part was eroded 500 m deeper than the eastern limb. The eroded surface was covered by basalts, the K–Ar age of which was estimated at  $6.3 \pm 0.3$  to  $4.3 \pm 0.2$  Ma (Trifonov et al., 2011). The basaltic hyaloclastites formed 5.4 ± 0.2 Ma ago under the effect of seawater are now located 260–300 m above sea level (Outline of Geology of Syria, 2000). In the axial part of the anticline, the basalts dated at 5.4–4.8 Ma have been raised to a height of 800 m. At the eastern limb of the fold, basalts are located 400 m lower. The coastal Lebanon Anticline underwent intense Pliocene–Quaternary uplift, as well (Gomez et al., 2006).

The comparative analysis of height, composition and age of the terraces of largest rivers of Syria dives more detailed estimates of the Quaternary uplift of different tectonic provinces of the region (Fig. 23). The accurate definition of ages of different stages of terrace formation gave a possibility to define average rates of incision in the river valleys using relative height of the terraces that correspond approximately to the rates of the Quaternary rise in different tectonic provinces of Syria during the Middle and Late Pleistocene. The rates are: ~0.22–0.28 mm/a in the El-Kabir River valley (the Coastal Range), ~0.08–0.13 mm/a in the Orontes valley and the Euphrates valley

upstream the Assad Reservoir (the mobile platform Aleppo Block) and  $\sim 0.025\text{--}0.03$  mm/a in the Euphrates valley downstream the Assad Reservoir (the south-western side of the Mesopotamian Foredeep) (Neotectonics, recent geodynamics and seismic hazard assessment of Syria, 2012; Trifonov, Bachmanov et al., 2012, 2014).

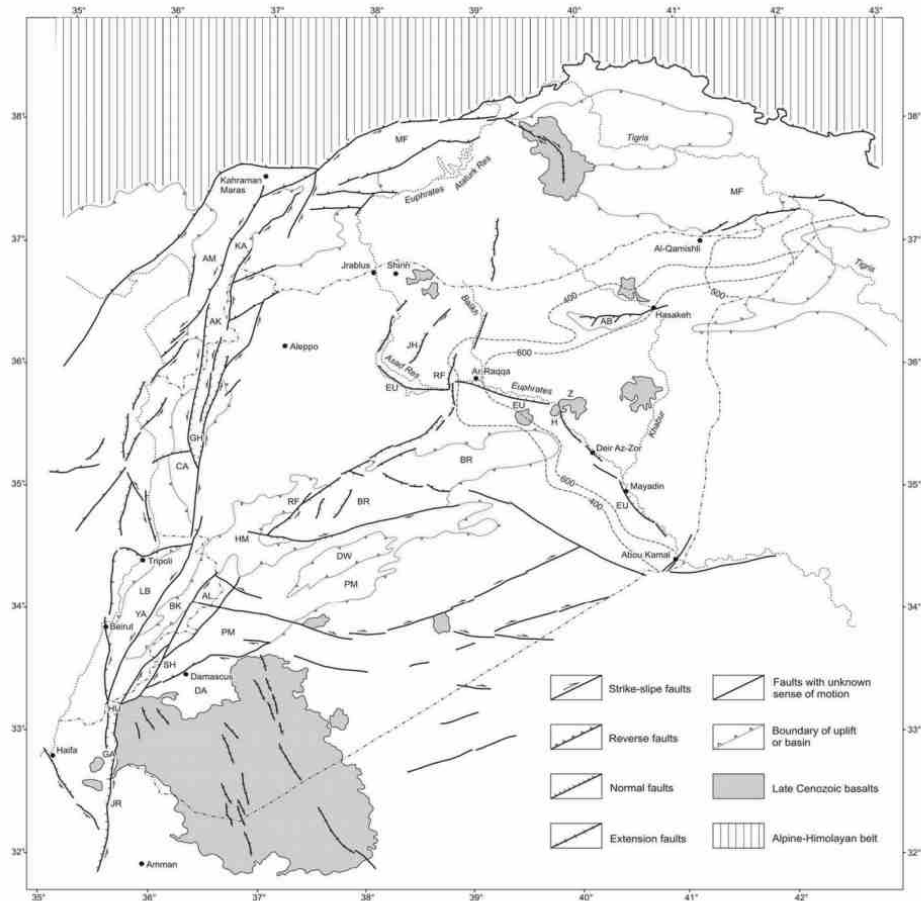


Fig. 22. Late Pliocene–Quaternary (the last  $\sim 3.5$  Ma) tectonic features of the northern part of the Arabian plate, modified after (Trifonov, Bachmanov et al., 2012). The 400-metre and 600-metre Miocene isopachs and the 500-metre Pliocene isopach demonstrate the structure of the Mesopotamian Foredeep. *Uplifted anticline zones*: AB, Abdel Aziz; AL, Antilebanon; BR, Bishri, the Northern Palmyrides; CA, Coastal of Syria; LB, Lebanon; MF, Marginal Folds of Turkey; PM, Southern Palmyrides. *Faults and fault zones*: AM, Amanos, a segment of the EAFZ; EAFZ, East Anatolian fault zone; EU, Euphrates; JH, Beer Jabel – Heimer Kabir; JR, Jordanian, a segment of the Dead Sea Transform (DST); RF, Rasafeh–Faid and its continuation (RF2, RF3 and RF4); SH, Serghaya; YA, Yammuneh, a segment of the DST. *Basins*: AK, Amik; BK, Bekkaa syncline; DA, Damascus; DW, Ad Daw; GA, Galilee Sea pull-apart basin of the DST; GH, El Ghab pull-apart basin of the DST; HM, Homs; HU, Hula pull-apart basin of the DST; KA, Karasu graben. Basaltic fields: H, Halabieh; Z, Zalabieh

Although the uplift of the mountain systems in the Pliocene and Quaternary involved most conjugate intermontane basins and foredeeps, some large negative structural elements in the western part of the belt underwent intense subsidence. Signs of this were found in the Mediterranean, Black Sea, South Caspian Basin, and in the southeastern part of the Terek Foredeep continuing into the Central Caspian as the Derbent Trough. The maximal thickness of the sedimentary cover exceeds 14 km in the Derbent Trough and the 5 km fall on the Pliocene–Quaternary deposits. The most intense sagging began at the end of the Pliocene and continues at present, providing uncompensated sedimentation (Leonov et al., 1998). The western part of the South Caspian is a starved basin down to 1 km deep with thinned (8–10 km) consolidated crust. Up to 20 km of sediments have been deposited here, no less than half of them being Pliocene–Quaternary sediments. The thickness of the Upper Pliocene–Quaternary deposits locally exceeds 6 km (Artyushkov, 1993; Leonov et al., 1998).

The subsidence of the Aegean Sea started in the Late Miocene and became more intense in the Pliocene and Quaternary (Golonka, 2004). At the same time, from the Tortonian and especially in the Pliocene–Quaternary, the Ionian and Levantine basins of the Mediterranean Sea also deepened. Increase of sagging of the latter from the Tortonian to Pliocene–Quaternary is confirmed by the growth of the sedimentation rate by 2–6 times in various parts of the basin (Kazakov, Vasilyeva, 1992). The Levantine Basin, uncompensated by sediments, is up to 2500 m deep (3200 m at the Herodotus abyssal plain). In the north of the basin, a trough in front of the Cyprus arc is expressed in the west as a deep bathymetric depression between the Cyprus and the submarine Eratosthenes Mount and in the east as a submarine extension of the Nahr el Kabir Trough, where the thickness of the Pliocene–Quaternary sediments is greater than 1800 m.

The Levantine Basin is a relic of the southern margin of the Tethys, which now has suboceanic crust with thick (up to 10–14 km) sedimentary cover and the Moho surface at a depth of 20–25 km (Ben-Avraham et al., 2002). The lower and the upper parts of the Neogene–Quaternary section are separated by the Messinian evaporites, which are replaced in the south by alluvial and deltaic sediments of the pra-Nile. The level of the hypersaline Messinian Basin was lower than the present-day level of the Mediterranean. This is proved by the overdeepening of the Messinian channels of the pra-Nile and the other rivers influent into the sea at that time. Currently evaporites occur at a depth of 2 km and deeper.

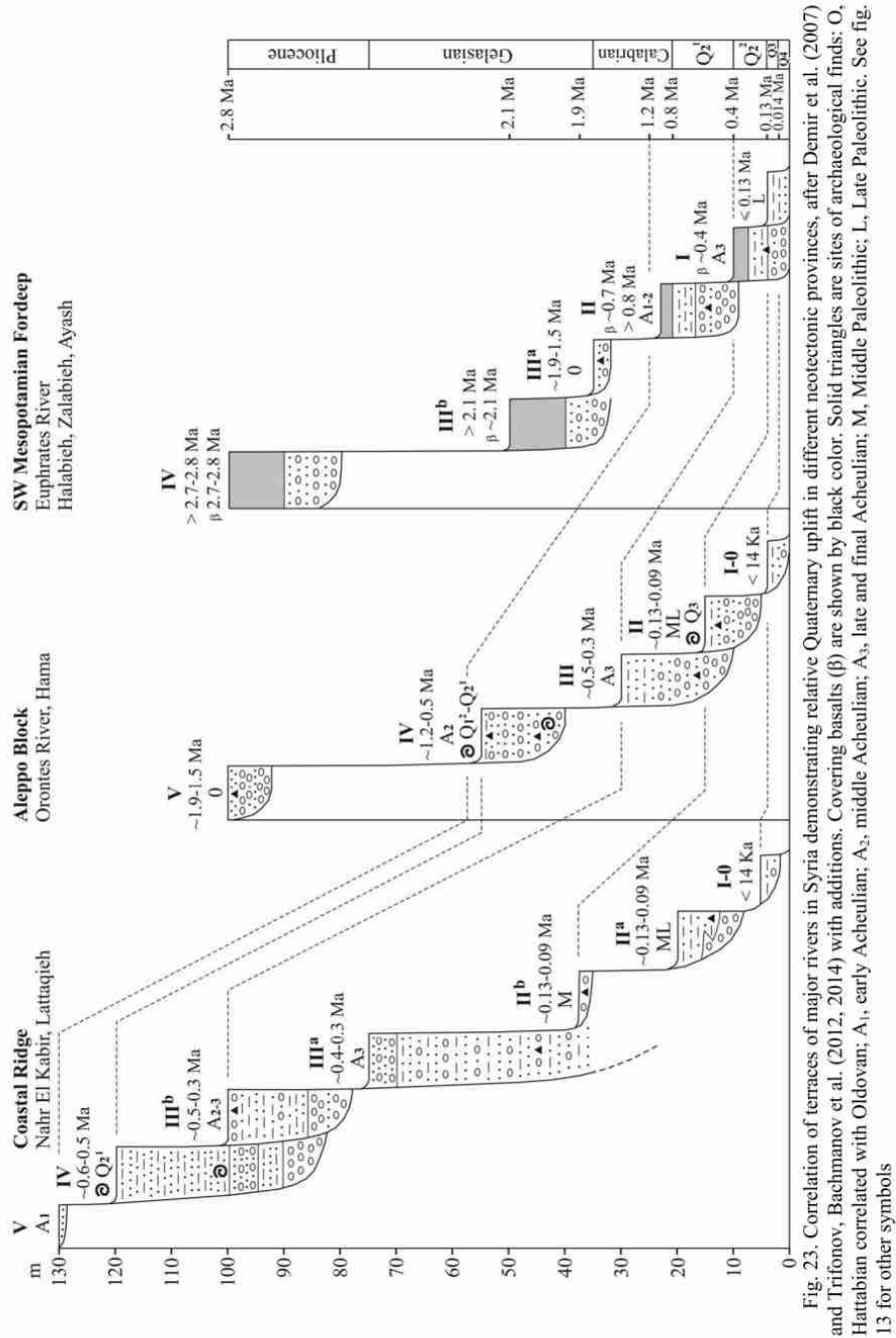


Fig. 23. Correlation of terraces of major rivers in Syria demonstrating relative Quaternary uplift in different neotectonic provinces, after Demir et al. (2007) and Trifonov, Bachmanov et al. (2012, 2014) with additions. Covering basalts ( $\beta$ ) are shown by black color. Solid triangles are sites of archaeological finds: O, Hattabian correlated with Oldovan; A<sub>1</sub>, early Acheulian; A<sub>2</sub>, middle Acheulian; A<sub>3</sub>, late and final Acheulian; M, Middle Paleolithic; L, Late Paleolithic. See fig. 13 for other symbols

In the Early Pliocene, the breaching waters of the Black Sea and Atlantic flooded the Mediterranean, including the Levantine Basin. The depth of its bottom decreases toward its eastern shore and especially southward, where a vast shoal is occupied by the Nile delta, in the underwater part of which the thickness of the Pliocene–Quaternary sequence reaches 3.0–3.5 km (Ross, Uchupi, 1977). At the boundary of the continental slope and the basin bottom between Tel-Aviv and Beirut, their thickness is 1.3 km (Ben-Gai et al., 2004) and the bottom of the Pliocene sediments is subsided to 2.2–2.4 km (Kazakov, Vasilyeva, 1992).

At the same time, in the west of Syria, in the subaerial part of the Nahr el Kabir Trough, the 30-m section of the Messinian gypsum is exposed at a height of ~50 m a.s.l. The Pliocene marine clay overlaps it with scouring and basal breccia containing fragments of gypsum and pre-Messinian carbonates and covers the slopes of the adjacent uplifts at a height up to 250 m. No indications of ingressive attitude of the Pliocene were revealed. The submarine part of the Nahr el Kabir Trough and the neighboring part of the continental slope are disturbed by faults, along which the trough stepwise plunges to the west (Klaeschen et al., 2005). The seismic profiles across the slopes of the Levantine Basin between Tel-Aviv and Beirut demonstrate that horizontally lying Pliocene–Quaternary sediments are thinned landward, forming a flexure on the continental slope with dip angles up to 10° and complicated by faults (Ben-Gai et al., 2004). The vertical offset of the Pliocene bottom reaches 1.5–1.7 km. The steepness of the beds decreases from the Pliocene to the Quaternary, however, even the Late Pleistocene (Tyrrhenian) terraces are locally tilted seaward at an angle of 3° (Dodonov et al., 2008).

The relationships described above show that the sea level in the Messinian was lower than the contemporary sea level by several hundred meters. The Tortonian carbonate rocks deposited in the very shallow-water sea occur now in the Nahr el Kabir River valley at a height no more than a few hundred meters. Thus, the Pliocene–Quaternary uplift of the shore was not great and became significant only in the coastal anticlinal ridges (Gomez et al., 2006). Thus, increase in the vertical contrast between the Early Pliocene surface on the present-day land and in the sea is determined largely by deepening of the Levantine Basin, which underwent tectonic subsidence with a magnitude no less than 1.5 km in the post-Messinian time. An additional isostatic subsidence related to load of thick sediments took place in the Nile delta.

Thus, the Pliocene–Quaternary was the time of activation of not only rising, but also subsiding tectonic movements, that is, the time of general increase in their contrast.

### **1.5.5. Relationships between collision and tectonic uplift producing mountain building**

The signs of the first orogeny in the Alpine–Himalayan belt are referred to the Oligocene. The mountain system became widespread in the Pliocene and Quaternary. The neotectonic epoch immediately followed, partly coinciding in time with the epoch of collision closure of the Neotethys and its backarc basins, which began at the end of the Cretaceous and completed in the time interval from the Late Eocene to Middle Miocene. The region of mountain building is juxtaposed, to a great extent, with the domain of collision, though it expands beyond the limits of collision in the east. This provides grounds to regard recent mountain building as a result of collision compression, and this view is generally accepted now. Let us consider to what extent this opinion is valid.

#### **1.5.5.1. Methodical Approach**

The occurrence and height of the uplifts, which towered above the sea level or the surface of the subaerial peneplain that existed earlier and is retained nearby, can be judged from the composition of clastic material removed from the eroded uplift and from the depth of the related incision onto the peneplain. When analyzing clastic material, it should be kept in mind that coarse facies could have been accumulated as a result of destruction of the overthrusting allochthonous sheets, which did not undergo substantial uplifting (Leonov M.G., 1975; Bachmanov et al., 2008). In some basins, clastic material was deposited as a product of remote transportation by water and does not characterize the height of the adjacent rises. All this requires ascertainment of the paleotectonic setting of sedimentation.

As concerns the depth of incision, in the case of intense linear erosion accompanying growth of mountain ranges, the remnants of the pre-orogenic surface can be retained on their summits and slopes, allowing judgment about the magnitude of uplift. The stepwise slopes of mountain ranges are commonly interpreted as evidence for pulsatory uplift and serve as the basis of the concept of step-like topography. Acceleration of vertical movements reactivates erosion so that an erosion–tectonic scarp (incision) is formed on the slope of the uplift, leaning on the bottom of the basin or valley, which serves as a local base level regulating deposition of erosion products. The higher the rate of uplifting, the coarser and thicker the accumulation of sedimentary material. The next pulse of rising leads to the uplift of an adjacent site of the basin and the formation of a younger incision below it. The uplifted site becomes a step on the slope. The steps located at similar hypsometric

levels on the slopes of different ranges make up, together with the incision leaning on them, a regional level of topography formed at the same time. This suggests that the incision is correlated with the coarse lower part of the molasse unit, whereas the steps at the base of incision are correlated with the fine clastic upper part of the molasse unit (Makarov, 1977). Such correlation gives a possibility to use molasse units as indicators of development of a mountain system and magnitudes of its uplift during different time intervals. In the course of intensive rise, the early landforms can be destroyed and the retained landforms will not reflect its true vertical uplift that can be controlled by analysis of the recent structure of a mountain range.

Thus, origination and growth of the mountain system is recorded in a complex of sedimentary, geomorphological and structural–geological attributes. The set of such attributes, while not allowing the identification of all features of regional mountain building, nevertheless gives an idea of the general tendencies of uplifting.

#### **1.5.5.2. Mountain building as a result of collision compression**

As was shown above (Fig. 1 and 16–18), the Alpine-Himalayan Belt underwent Cenozoic transverse shortening under the effect of collision compression. The process was accompanied by rotation of separate microplates (Kopp, 1997). The orientation of the compression axis changed with time. At the first substage of the stage 1 (Oligocene–Early Miocene), the NNW orientation was predominant; during the second substage (late Early–Middle Miocene) it was oriented in the NE direction; at the third substage (Late Miocene–Early Pliocene), the orientation again was NNE or N–S. The N–S-trending compression dominated during the stage 2 (Late Pliocene–Quaternary).

The geodynamic correlation is outlined between the tectonic events at the northern flanks of the Arabian Plate and the evolution of the Aden–Red Sea Rift System (Kazmin, 1974; Rukieh et al., 2005; Trifonov et al., 2011; Neotectonics, recent geodynamics and seismic hazard assessment of Syria, 2012). At the first substage, the rift system propagated westward and the Aden Rift pulled apart more intensively than the Red Sea Rift. The Arabian Plate correspondingly moved to the north-northwest. At the second substage, the Red Sea Rift extended more intensely than the Aden Rift and the Arabian Plate moved to the northeast. During the third substage, the intensity of extension increased because of the breakup of the continental crust and the onset of spreading (Kazmin, 1974; Izzeldin, 1987). Inasmuch as the breakup of the crust and spreading developed in the Aden Rift earlier than in the Red Sea Rift, the plate

moved to the north-northwest. Finally, at the stage 2, the Red Sea Rift was involved in spreading as well, and the plate began to move northward.

As was shown above, similar variations of orientation of the compression axis also took place in other segments of the orogenic belt, which were not related to the drift of the Arabian Plate. It is obvious that they were controlled by more general geodynamic factors that caused the drift of Arabia among other phenomena.

In contrast to the above variations of the stress-and-strain state, the propagation of the Zagros Fold Belt to the SW was characterized by the stress state that remained unchanged over all stages of its evolution. This is indicated by the parallel orientation of folds differing in age and the conjugated NW-trending thrusts. In contrast to the folds, the structural framework of the Zagros as the right lateral Main Recent Fault is inscribed into the setting of near N-trending compression established in the Pliocene–Quaternary. At that time, the Main Fault was separated from the zone of active folding by previously formed fold zones, where folding ceased. The stress fields different in rank are probably combined here. The transregional field controlled by common movement and interaction of lithosphere plates and microplates caused dextral movements on the Main Fault. The regional field involving only the Zagros caused deformation on the fold-thrust Zagros Belt. Appearance of this regional field may be due to the wedge shape of the Arabian Plate, which creates compression of its northeastern margin in the process of the northward drift. A similar propagation with the same geodynamic consequences took place in the Himalayas, where the front of the maximal displacement and deformation migrated in the post-Middle Miocene time from the Central Thrust Fault to the Boundary and then Frontal faults and now is shifting to the Sub-Himalayas.

From the Late Eocene to the Early Pliocene, the uplifts expressed in the topography arose and developed in the same tectonic zones of the belt, which underwent the strongest compression and shortening. Such uplifts can be regarded as a result of isostatic compensation of thickening of the crust due to its compression. Differentiation of the peneplain with the formation of uplifts and intermontane basins took place also beyond the regions of collision diastrophism expressed in folding and thrusting, e.g., in the Central and Eastern Tien Shan. Its compression could have been induced by the movements of microplates in the course of collision. In the Tien Shan, this was the pressure of the Tarim microplate. Because the direction of principal compression varied during the Oligocene–Quaternary epoch, the uplifts differing in strike originated at different times. The growth of mountains could last after the onset of diastrophism, probably, owing to inertia of isostatic compensation.

The height of the mountain ranges was estimated in two ways: first, using the geologic–geomorphic method discussed above, and second, by calculation based on correlation between rise of the crust and its deformational shortening with using equations (1) and (2) (see section 1.2.3). The value and rate of shortening and corresponding initial width of the region were estimated from structural–geological data, whereas the initial thickness of the crust was estimated from its thickness in the adjacent undeformed regions with similar initial characteristics of the crust that is possible to do for the Tien Shan and Himalayas, or on the basis of geological features, if the region under consideration initially differed from the adjacent territories (the Greater Caucasus, Pamirs, Zagros).

Calculation of isostatic uplift since the Oligocene as a result of thickening of the crust by compression made by Artyushkov for the Central Tien Shan has shown that by the end of the Pliocene (onset of intense rising), the uplift reached 0.6–0.9 km (Trifonov et al., 2008; see section 1.2.3). This estimate is consistent with geologic–geomorphic estimates, according to which the height of the uplift by the end of the Pliocene did not exceed 1.5 km; the difference in the heights of the uplifts and the surface of the basins was 1 km and the average height of the Central Tien Shan was close to 1 km, i.e., ~0.7 km higher than the height of the initial pre-orogenic peneplain (see section 1.2.1). In other words, before intensification of mountain building, the growth of uplifts could be entirely determined by regional compression.

The characteristics of the molasse formations and rare estimates of correlative incisions into the planation surfaces and pediplanes in other mountain systems of the belt lead to similar conclusions. The uplifts, which arose from the Oligocene up to the Pliocene or Early Pliocene, aside from occasional local deviations, also towered above the pre-orogenic peneplain by not more than ~1.5 km, i.e., they were not higher than middle-level mountains. It is quite possible that they were created by thickening of the crust owing to compression. In the Eastern Carpathians and the Southern Slope Zone of the Greater Caucasus, the deformational thickening of the crust in the Middle–Late Miocene did not result in the corresponding rise of the territory. In the Carpathians, the cause could have been related to compaction of the lower crust (Artyushkov et al., 1996). A similar situation probably took place in the Greater Caucasus. The formation of the Pannonian Basin also could be caused by an increase in the lower crust density.

The transverse segmentation of the belt is clearly expressed in its contemporary structure. The eastern Pamir-Himalayan segment separated from the central Caucasus-Arabian-Iranian segment by the Darwaz–Chaman Fault System is

characterized by a maximum of rising that involves not only mountain systems, but also most conjugated basins and plains (microplates). This feature of the eastern segment was retained through the entire neotectonic epoch, increasing with time. Cenozoic granitic magmatism is widespread here, whereas in other segments granites are not so abundant in contrast to the intense recent volcanic activity. The central segment, separated from the western one by the Dead Sea Transform and East Anatolian Fault Zone, is characterized by more differentiated topography. The mountain systems here are lower than in the east, and the Caspian Basin and Persian Bay are situated at the periphery of the belt. The area of intensive recent volcanism extends along the western margin of the segment. In the western segment, mountainous domains are combined with basins. Both rising of mountains (the Alps, the Carpathians, Anatolia) and subsiding of basins were intensified here.

It would be suggested that the topographic features of the segments are related to different rates of their compression, or transverse shortening. It actually reaches a maximum in the eastern segment owing to substantial displacement of the Indian Plate; however, in the same segment, the highest tectonic uplift took place in the Himalayas rather than in the Punjab–Pamir arc, where shortening was highest. It is evident that differences in the intensity of vertical movements were related not only to intensity of compression, but also to the features of the lithosphere determined by the tectonic history and deep geodynamics.

#### 1.5.5.3. Pliocene–Quaternary acceleration of tectonic uplift producing mountain building

The Pliocene–Quaternary mountain building fundamentally differs from the preceding stages of the evolution of the orogenic belt not only in the higher intensity of uplifting, but also in the extensiveness of the involved territories irrespective of their tectonic history. The uplifts embraced the whole of Central Asia and developed in other regions of the belt.

The intensification of Pliocene–Quaternary rising is only partly related to acceleration of plate movements and increase in collision compression. On the contrary, the intensity of compression locally decreased. For example, in the Alps and the Western Carpathians, collision was completed as early as the Middle Miocene, whereas the mountains began to grow in the Pliocene against the background of diminished compression. In the Greater Caucasus, the growth of uplifts accelerated in the Pliocene–Quaternary against the background of decreasing compression rate

recorded in the GPS data (Shevchenko et al., 1999) and total displacement along active faults (Trifonov et al., 2002). Even in the regions, where compression increased (Himalayas, Pamir, Central Tien Shan), the magnitudes of uplifting related to the thickening of the crust by compression are only a part of the total magnitude of the uplift over this time (Fig. 6). If the compression rate in the Central Tien Shan estimated from the data on Late Quaternary displacements along faults and the results of GPS measurements (10–20 mm/yr) is extrapolated over the entire phase of intense mountain building (Late Pliocene–Quaternary), then it will be higher than the average compression rate in the preceding epochs (2.5–3.0 mm/yr). The isostatic uplift at this rate of crust compression estimated from formula (1) is 330–660 m, i.e., 20–35% of the increment of average height of mountain edifice of ~2–2.5 km (Trifonov et al., 2008; see section 1.2.3). A similar calculation of the height increment of the Himalayas and Pamir in the Pliocene and Quaternary yielded no more than 40–50%. Most intermontane basins rose also, though not so intensely, and this hardly can be a manifestation of compression. Thus, regardless of either increase or decrease of regional compression in the Pliocene and Quaternary, this factor may explain only a part of the rate of uplifting, and not everywhere. The remainder must be explained by the contribution of other factors.

The tectonically delaminated lithospheric mantle including the high-metamorphosed fragments of the lower crust was partly replaced by the lower-dense asthenosphere (Artyushkov, 1993, 2003; Trifonov et al., 2008), and this abruptly intensified the growth of mountain ranges. This is indicated by the lowered seismic wave velocities beneath the highest mountain systems of Central Asia (Himalayas, Tibet, Kunlun, Pamir–Hindu Kush–Karakoram region, Central and Eastern Tien Shan) (Lukk, Vinnik, 1975; Lithosphere of the Tien Shan, 1986; Recent geodynamics..., 2005; Vinnik et al., 2006; Li Zhiwei et al., 2009), as direct evidence for the low-density upper mantle suggested from gravity measurements (Artemjev, Kaban, 1994; Jimnez-Munt et al., 2008). Kaban (2000) noted the same features in the gravity field of the Lesser Caucasus. The lowered seismic wave velocity related to the ascent of the asthenosphere was revealed beneath the Eastern Carpathians (Artyushkov et al., 1996). The decrease of density of the lower crust masses as a result of retrograde metamorphism under the effect of cooled Pliocene asthenosphere fluids may be the second factor of intensification of mountain growth. This factor probably became dominant in the uplift of the Western Tien Shan and the Greater Caucasus, where low-density mantle domains have not been detected except for the Elbrus magma source.

### 1.5.6. Sources of neotectonic uplift in the Alpine-Himalayan Belt

In the Cenozoic, especially since the Late Eocene, different zones of the Alpine–Himalayan Belt have undergone collision compression caused by convergence of the Gondwanan plates with the Eurasian Plate. This compression was expressed in folding, thrusting of the sheets of continental crust over one another, and closure of the Neotethyan basins and related backarc seas and eventually led to the local thickening of the crust and its isostatic uplifting. The uplifts that grew in such a way, as a rule, did not exceed the hypsometric level of low and moderately high mountains. The process continued like this up to the Early Pliocene and the areas occupied by uplifts became more extensive with each new tectonic phase. In other words, before the Early Pliocene, the growth of mountain systems was almost completely caused by collision compression of the belt, although local deviations from the isostatic compensation of compression arose, being directed toward the greater magnitudes of uplift, e.g., in the eastern segment where low-density granites were formed, and to the lower magnitudes in the Eastern Carpathians and the Greater Caucasus, probably due to metamorphic compaction of the lower crust.

The isostatic uplifting of the crust thickened by compression developed further in the Pliocene–Quaternary, locally even more intensively than before, but general rising of most part of the orogenic belt was added to this process. The general rise was greater in magnitude than the contribution of the uplift caused by local thickening of the crust by compression; it did not depend on the Cenozoic history of either territory, involved not only mountain ridges, but also the majority of adjacent basins, and eventually led to the formation of the contemporary mountain topography of the belt. This additional rise was caused by decrease of density of the uppermost mantle and the lower crust. The isostatic reaction to the decrease of density of the upper mantle was a result of partial replacement of the lithospheric mantle with the asthenosphere material, whereas the decrease of density of the lower crust was due to retrograde metamorphism under the effect of cooled asthenosphere fluids. The deep transformations also caused deepening of some basins and increased contrast of transverse segmentation of the belt.

## Part 2. Result of seismic tomography analysis of the mantle and deep sources of the Pliocene–Quaternary uplift

### 2.1. Seismic tomography profiling of the Alpine-Himalayan Belt

Consideration of the seismic tomography data on northeastern Asia (Zhao et al., 2010) has shown that the processed data from the global network of stations, though worse in resolution compared to the data of the regional seismological network, nevertheless give a generally similar pattern. Therefore, the seismic tomography data obtained on the basis of the global network were used for the study of the Ethiopian–Afar superplume and the Alpine–Himalayan Belt (Grand et al., 1997; Van der Hilst et al., 1997; Becker, Boschi, 2002). When these data are interpreted, their lower spatial resolution in comparison with the regional models should be kept in mind. In particular, this resolution does not allow discrimination of the lithosphere and asthenosphere. Other geophysical evidence is needed for this purpose. For example, the lower average seismic wave velocities beneath continents at a depth down to 100 km are interpreted as evidence for emergence of the asthenosphere.

The lines of the seismic tomography sections are shown in maps of  $V_p$  and  $V_s$  variations in the surface layer 100 km in thickness (Fig. 24 & 25). The sections themselves (Fig. 26–29) are based on these data (Grand et al., 1997; Van der Hilst et al., 1997; Becker, Boschi, 2002). The anomalous  $V_p$  and  $V_s$  values are expressed in percent as deviations from the average value for the given layer. The  $dV_p = 0.25–0.8\%$  and  $dV_s = 0.5–2.0\%$  are accepted as increased and  $dV_p > 0.8\%$  and  $dV_s > 2\%$  as highly increased. By the same way, the  $dV_p = -0.25–0.8\%$  and  $dV_s = -0.5–2.0\%$  are accepted as lowered and  $dV_p < -0.8\%$  and  $dV_s < -2\%$  as highly lowered. Systems of mid-ocean ridges are distinctly seen in the  $V_s$  field with two exceptions. They are the Knipovich Ridge and a segment of the African–Antarctic Ridge near the Kerguelen Plateau. At the same time, systems of mid-ocean ridges are not expressed almost at all in the  $V_p$  field. In contrast, the collision zones of the Earth, in particular, the Alpine–Himalayan Belt, are clearly seen in the  $V_p$  field.

Sections 1–1' across the Tonga–Kermadec arc show that the zone of increased and highly increased  $dV_s$  corresponding to the seismic focal zone transforms at a depth of 400–800 km into the horizontal high-velocity lens beneath the sub-continental Tonga

Plain (Fig. 26). A similar passage is revealed beneath the Andaman–Indonesian arc (Fig. 26, sections 2–2'). Similar flattening of subduction zones has been found at the depths of 400–700 km along the north-western margin of the Pacific by the more detailed data of local seismic networks. Fukao et al. termed this layer a stagnant slab and Huang and Zhao (2006), Zhao (2009) and Zhao et al. (2010) termed it a big mantle wedge (BMW) (Fig. 26, sections 20 and 24).

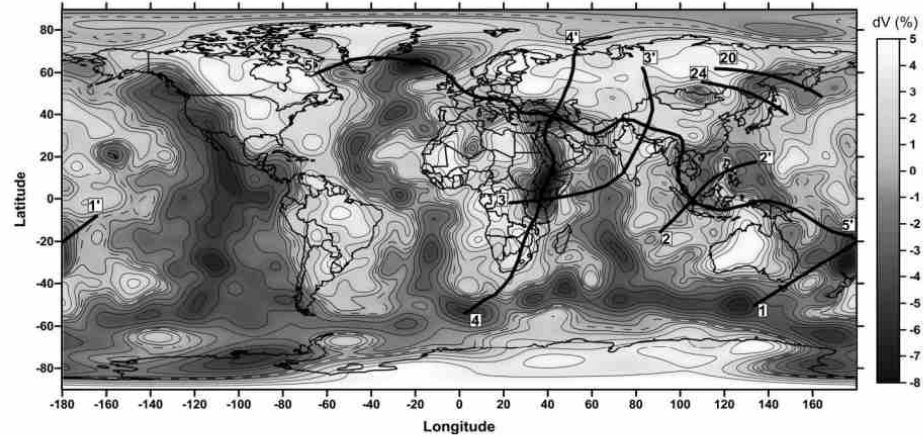


Fig. 24. Distribution of  $dV_S$  at the depth up to 100 km and lines of sections (Fig. 26–29), lines 20 and 24 after (Zhao et al., 2010). Compiled after the data in (Becker, Boschi, 2002; Grand et al., 1997; Van der Hilst et al., 1997). Contour lines are spaced at 1%; the dashed line corresponds to zero value

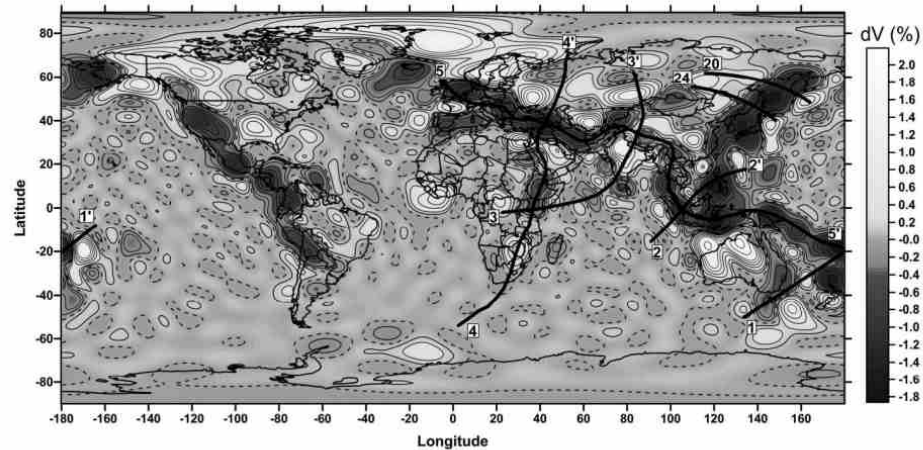


Fig. 25. Distribution of  $dV_P$  at the depth up to 100 km and lines of sections (Fig. 26–29), lines 20 and 24 after (Zhao et al., 2010). Compiled after the data in (Becker, Boschi, 2002; Grand et al., 1997; Van der Hilst et al., 1997). Contour lines are spaced at 0.2%; the dashed line corresponds to zero value

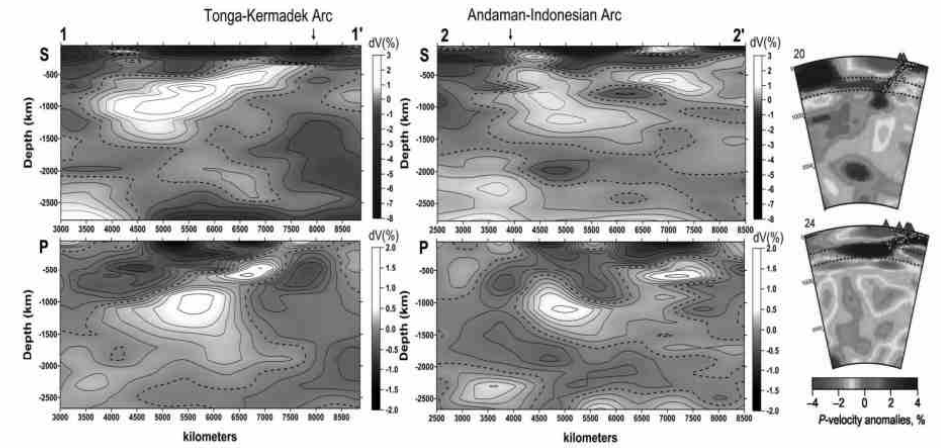


Fig. 26. Seismic tomography  $dV_P$  and  $dV_S$  sections along lines: 1–1' across the Tonga-Kermadec Arc; 2–2' across Philippines and the Andaman-Indonesian Arc. Compiled after the data in (Becker, Boschi, 2002; Grand et al., 1997; Van der Hilst et al., 1997). Contour lines are spaced at 0.25% for  $P$ -waves and 0.5% for  $S$ -waves; the dashed lines correspond to zero value. The  $dV_P$  profiles across Kamchatka (20) and Khokaido (24) after (Huang, Zhao, 2006; Zhao, 2009; Zhao et al., 2010) are given for comparison. Small white circles are hypocenters of earthquakes and dark triangles are volcanoes in the profiles 20 and 24. See fig. 24 and 25 for position and legend

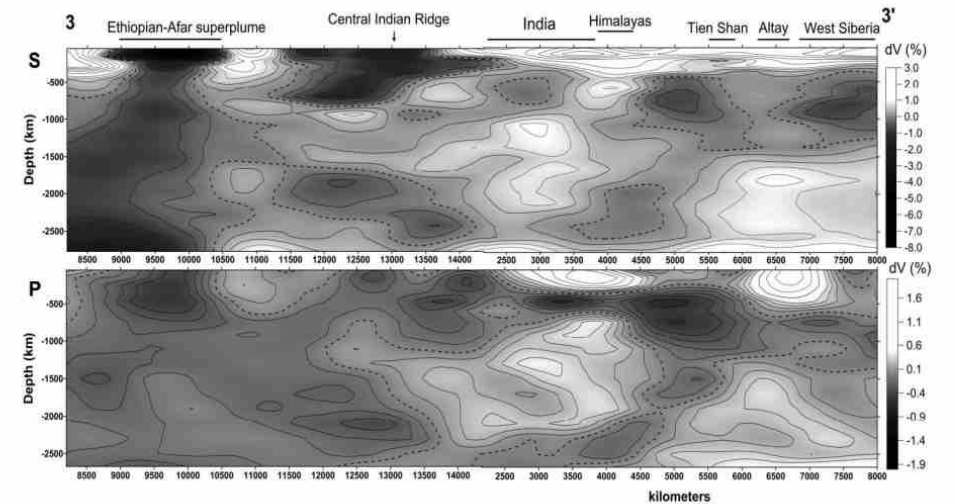


Fig. 27. Seismic tomography  $dV_P$  and  $dV_S$  sections along line 3–3' from Kenya via the Mid-Indian Ridge, Indian Platform, and High Asia to the post-Paleozoic West Siberian Platform. Compiled after the data in (Becker, Boschi, 2002; Grand et al., 1997; Van der Hilst et al., 1997). Contour lines are spaced at 0.25% for  $P$ -waves and 0.5% for  $S$ -waves; the dashed lines correspond to zero value. See fig. 24 and 25 for position and legend

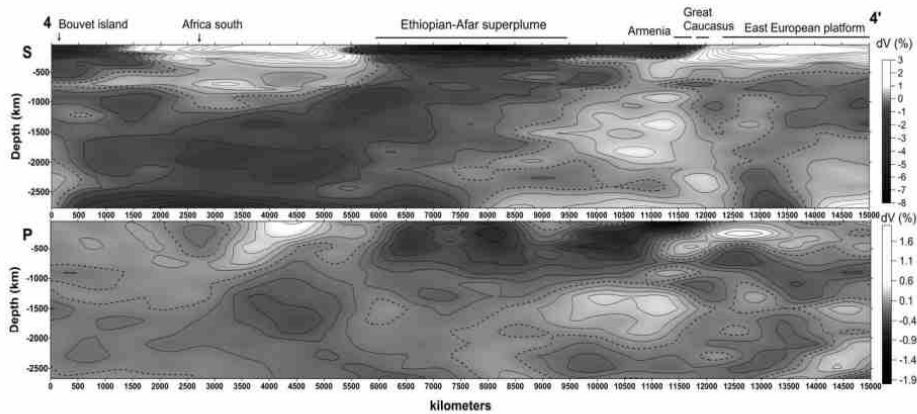


Fig. 28. Seismic tomography  $dV_p$  and  $dV_s$  sections along line 4–4' from South Africa via the Ethiopian-Afar super-plume, Arabian Platform and the Caucasus to the East European Platform. Compiled after the data in (Becker, Boschi, 2002; Grand et al., 1997; Van der Hilst et al., 1997). Contour lines are spaced at 0.25% for  $P$ -waves and 0.5% for  $S$ -waves; the dashed lines correspond to zero value. See fig. 24 and 25 for position and legend

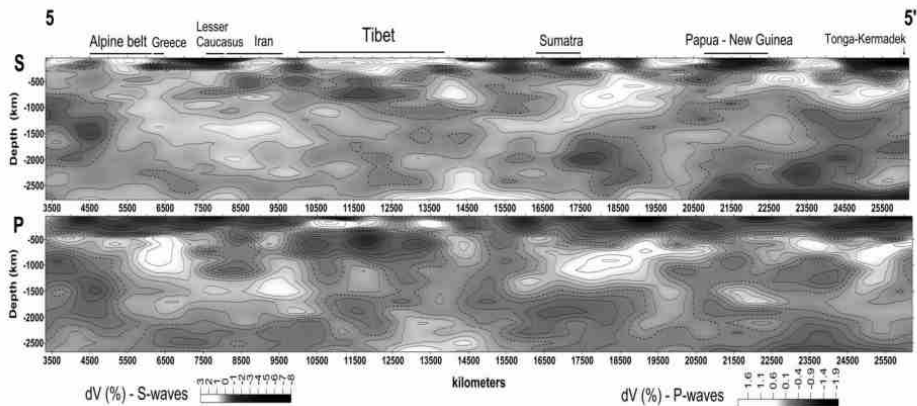


Fig. 29. Seismic tomography  $dV_p$  and  $dV_s$  sections along line 5–5' along the Alpine-Himalayan Belt from Tonga-Kermadec Arc via the Indonesian back-arc basin, Tibet, Pamirs, the Lesser Caucasus, Anatolian Plate, and the Carpathians to the West European Hercynides. Compiled after the data in (Becker, Boschi, 2002; Grand et al., 1997; Van der Hilst et al., 1997). Contour lines are spaced at 0.25% for  $P$ -waves and 0.5% for  $S$ -waves; the dashed lines correspond to zero value. See fig. 24 and 25 for position and legend

Another situation is characteristic of the Tibetan–Himalayan segment of the belt (Fig. 27, section 3–3'). The layer of highly increased  $dVs$  down to the depth of 100–300 km extends here from the Himalayas to the northern margin of the Tien Shan and continues as a high-velocity layer beneath the Indian Platform and the Kazakhstan–

West Siberian segment of the Eurasian Plate. The high-velocity layer thickens to 400 km beneath Southern Tibet near the Neotethian Suture (Indus–Zangpo Zone). One more nearly horizontal high-velocity lens is detected there at a depth of 600–700 km.

It cannot be ruled out that a part of the upper high-velocity layer and this lens are transformed relics of the Neotethyan slab flattened at a depth. In the  $dV_p$  section, a similar high-velocity lens is traced from the southern margin of the Indian Platform to the northern margin of Tibet at a depth of 100–300 km. The greatest thickness of this layer and the highest  $dV_p$  values are established beneath Southern Tibet. To the north, the averaged  $dV_p$  values in the upper mantle decline to a moderate level and one more high-velocity lens appears in the south of Western Siberia. A domain of lowered  $dV_p$  occurs below the high-velocity layer as a narrow (400–500 km) lens beneath the Indian Platform. This domain is reduced beneath Southern Tibet and swells to a depth of 300–800 km beneath High Asia from Tibet to the Tien Shan, where locally reaches very low  $dV_p$  values. In the lower mantle, a poorly delineated and fragmented zone of slightly lowered  $dV_p$  values tilted to the southwest occurs beneath this thickened lens. In the  $dV_s$  section, the above-mentioned features are less distinct. A domain of slightly lowered  $dVs$  values is situated beneath High Asia, and the tilted zone in the lower mantle is noted by moderate  $dVs$  against the background of slightly increased values beneath the adjacent territories.

Of principal importance are the seismic tomography sections across Africa, Arabia and the Arabian–Iranian segment of the Alpine–Himalayan Belt (Fig. 28, sections 4–4'). Relatively thin upper mantle lenses with highly lowered  $dVs$  values are seen in the section no deeper than 200 km. These are a short lens near Bouvet Island and a long lens, which extends beneath the East African Rift System and the Red Sea Rift to southern Arabia. The northern lens extends northward to the Greater Caucasus, where it is characterized by lowered  $dVs$  values. A wide domain of lowered and slightly lowered  $dVs$  values is traced below down to the bottom of the mantle. The upper part of this domain corresponds to the territory from Malawi to the Red Sea, and, being tilted to the south, is located beneath South Africa at the lower-mantle level. This domain is regarded as the Ethiopian–Afar superplume. The upper mantle of the African and Eurasian plates is distinguished by increased  $dVs$  values. A high-velocity wedge plunges from the Scythian Platform beneath the Greater Caucasus, where it flattens and is traced to the Lesser Caucasus, gradually losing its specificity. In the  $dV_p$  section, the Ethiopian–Afar superplume is also expressed as a wide domain of lowered  $dV_p$  values tilted to the south. In the upper mantle, this domain is traced to a depth of 600–800 km from Malawi to the Lesser Caucasus. Its segments

beneath the Kenyan Rift, Afar, and the Armenian Highland are distinguished by highly lowered  $dVp$ . Beneath the Greater Caucasus the thickness of this domain is abruptly reduced and limited from below by the high-velocity wedge plunging from the Scythian Platform. The upper mantle of South Africa and the East European Platform is characterized by slightly increased and medium  $dVp$  values.

The transverse sections are supplemented by longitudinal sections 5–5' oriented along the axis of the Alpine–Himalayan Belt and extending from the Tonga–Kermadec arc via the backarc basins of the Andaman–Indonesian arc, Tibet, the Pamirs, Afghanistan, Iran, and the Lesser Caucasus to Anatolia and via the Carpathians to the West European Hercynides (Fig. 29). These sections are important for understanding of the deep structure of the belt for two reasons.

First, they make it possible to look at the structures delineated in the transverse sections in another perspective. For example, the longitudinal sections confirm passing of the slab beneath the Tonga–Kermadec arc in a nearly horizontal zone of increased  $Vp$  and  $Vs$  values at a depth of 600–800 km. In the  $dVs$  section, this zone is supplemented by nearly horizontal high-velocity lenses at depths of 100–200 and 350–500 km at the western Pacific margin and at a depth of ~200 km between the Papua New Guinea arc and the eastern flank of the Andaman–Indonesian arc. The two-floor structure of the upper mantle beneath Tibet (increased  $Vp$  above and lowered  $Vp$  below) revealed in transverse section 3–3' is confirmed by the longitudinal section, where such a structure is detected over the entire territory from the eastern margin of Tibet to the Pamir–Hindu Kush. In the west, from Afghanistan to the Carpathians, a layer of lowered and highly lowered  $dVp$  values is depicted at a depth down to 200–300 km and extends beneath the West European Hercynides. The fact that the same structures are detected in both longitudinal and transverse sections indicates that the revealed variations are related to real mantle inhomogeneities rather than to the effect of anisotropic propagation of seismic waves.

Second, sections 5–5' demonstrate segmentation of the belt known from the relationships between the Late Cenozoic crustal structural elements (Trifonov et al., 2002). This segmentation is expressed better in the  $dVp$  section, where the difference of the segments is traced throughout the upper mantle. The boundary between the southeastern island-arc and the Tibetan section types approximately coincides with the fault zone of 105°E between the corresponding segments of the belt, whereas the boundary between the Tibetan and the Iran–Caucasus section types fits the Darwaz–Chaman Fault Zone between the Pamir–Himalayan and the Arabian–Iranian segments.

## **2.2. A model of structural evolution of the mantle beneath the Tethys and Alpine-Himalayan Collision Belt in Mesozoic and Cenozoic and its geological consequences**

### **2.2.1. Ethiopian-Afar superplume and upper-mantle flows spreading away from it**

Two structural features are the most important in the described above results of the seismic tomography profiling. First, the subduction zones flatten in the level of the transitional layer of the mantle (approximately 400–700 km) and form the BMW zones in the Indonesian segment of the Alpine-Himalayan Belt, where the subduction continues till now. Second, in the more northwestern Himalayan-Tibetan and Arabian-Caucasus segments of the belt, where the subduction finished in the time interval between the late Middle Eocene and Middle Miocene with a closure of the last relics of the Neothetys, the thick layer of the sub-lithosphere mantle with lowered seismic wave velocities extends uninterruptedly from the Ethiopian-Afar superplume (Sokolov, Trifonov, 2012).

Studying the Aleutian, Kurile–Kamchatka and Japanese island arcs, Huang and Zhao (2006) and Zhao et al. (2010) has shown that only in 5 of 22 transverse sections do slabs extend below 670 km. In other sections, slabs pass into a sub-horizontal layers at a depth of 410 to 670 km. In the cases when slabs go deeper, this layer is also detected in the section and is expressed in the  $Vp$  field better than the downward continuation of the slab (Fig. 26, sections 20 and 26).

Formation of the BMW structures had important geological consequences. Anomalies of seismic wave velocities (deviations from average statistical values characteristic of certain depths) corresponding to ascending hot and descending cold mantle flows reach a few percent only in the asthenosphere and local segments of subducted slabs. Elsewhere in the mantle, they are lower, deviations of 0.25% for  $Vp$  and 0.5% for  $Vs$ , i.e., 0.02–0.06 km/s, deemed to be significant. At the same time,  $Vp$  in the mantle increases with depth from ~8 to ~13 km/s and  $Vs$  from 4.3 to 7.0 km/s. At certain levels, the velocities change by fractions of km/s. Such jumps are referred to variations in rock density, which cannot be caused only by increase or decrease of density of rocks under the load of overlying rocks, but suggest a change in the crystal structure of minerals.

These transformations, confirmed by laboratory experiments at super-high pressure and temperature, have been described in the literature and recently summarized in (Pushcharovsky Yu., Pushcharovsky D., 2010). These publications rid us from the necessity of detailed discussion in this book. Note only that at a depth of 50–100 km pyroxenes of mafic and ultramafic rocks are transformed into garnets with a higher density. Several other seismic discontinuities are detected below in the upper mantle. The most distinct and extensive boundaries occur at depths of ~410 and ~670 km. The ~410-km discontinuity corresponds to the transition of orthorhombic olivine to the variety with spinel structure (wadsleyite transformed at a depth of ~520 km into ringwoodite), the density of which increases by 8%. Clinopyroxene is transformed into wadsleyite and stishovite at approximately the same depth. Within a depth interval of 410 to 500 km, pyroxenes acquire a more compact ilmenite-type structure. Thus, garnet, spinel, and silicates with ilmenite structure dominate at a depth of 410–670 km. At a greater depth, these minerals are replaced by denser perovskite-like phases occupying ~80% of the volume of the lower mantle (Pushcharovsky Yu., Pushcharovsky D., 2010).

The aforesaid shows that the jumps at seismic discontinuities and partly the general increase in the seismic wave velocity with depth are caused by modification of the crystal structure of mantle minerals, while the bulk chemical composition remains rather uniform. The variation in velocity probably reflects variation in the mantle density with depth. The descending and ascending flows of the mantle material are traced through the aforementioned seismic boundaries, and this implies that the flows undergo the same change in mineral composition as the surrounding mantle, retaining a difference in temperature. Because of the temperature difference, the transition of olivine into a spinel phase, as well as of pyroxene with segregation of stishovite, proceeds in a cold slab at a lower pressure at a depth of 300–380 km. In hot superplumes, the depth of transition probably increases. It should also be kept in mind that phase transitions may be exothermic, e.g., transformation of olivine into spinel or pyroxene into the phase with ilmenite structure, or endothermic, for example, transition to perovskite-type structure (Sorokhtin, 2007), with additional complication of the seismic tomography patterns.

The water content in the asthenosphere is a principal parameter determining its geodynamic role. Ringwood (1975) estimated the water content at 0.1%. According to the data published by Pugin and Khitarov (1978), the water content in the mantle is measured by 0.1%. Green et al. (2010) showed that the water content decreases 2–3 times from subduction zones to spreading zones. At the same time, Letnikov (1988,

2003<sub>1,2</sub>) supposes that deep fluids play an important role in the formation of lithospheric (including crustal) magma sources and in metamorphism of the lithosphere. He suggests that the asthenosphere is the main source of fluids and also assumes that they may be supplied from a greater depth (Letnikov, 2001, 2006).

According to petrological and geochemical data, most minerals in the sublithosphere mantle are anhydrous (Ryabchikov, 2005). Only the rocks within the depth interval 410–670 km (a transitional layer of the mantle) may be an exception. The crystal structure of wadsleyite and ringwoodite allows replacement of a part of the oxygen anions in these anhydrous minerals with a hydroxyl group (Smyth, 1994; Jacobsen et al., 2005). The subducted slabs, which contain incompletely dehydrated amphibolites and metasedimentary rocks, can be a source of hydroxyl. As was shown above, such slabs are transformed into almost horizontal high-velocity lenses at a depth of 410–670 km (Otani, Zhao, 2009). The appreciable attenuation of shear waves along with insignificant change of their velocities (Lawrence, Wysession, 2006) and increased electric conductivity (Kelbert et al., 2009) indicate that fluids occur at those depths. As concerns deeper sources of aqueous fluids, recent data on the density of the Earth's core allows the occurrence of hydrogen therein. Iron hydride is stable at the temperature and pressure characteristic of the lower mantle (Pushcharovsky Yu., Pushcharovsky D., 2010), but the minerals of the lower mantle contain a minimal amount of oxygen, and this rules out its coupling with hydrogen. Such a possibility appears only at the depth interval 410–670 km. Thus, the transitional layer is the main potential source of water fluids in the mantle.

The Ethiopian-Afar superplume is a vast N-trending zone corresponding in the lithosphere level to the entire East African Rift System and continuing southward of the latitudes of Madagascar in the south (Fig. 30). The flows of the upper mantle material spread from the superplume up to the northern margins of the Alpine-Himalayan Belt. The trails of sublithosphere flows are marked in the seismic tomography sections across the Arabian-Iranian segment of the belt by the decreased seismic wave velocities throughout the entire upper mantle, the flow being seen better in the  $dV_p$  section (Fig. 28 & 29). The flow trails are also seen in the  $dV_p$  section 3–3' (Fig. 27), where the flow layer underlies the thin lithosphere of the Indian Ocean and is covered farther to the north by the high  $dV_p$  lens corresponding to the thickened lithosphere of the Indian Platform and High Asia. Beneath the flow layer, within the lower mantle, the zone of weakly lowered  $dV_p$  values is found. Like the Ethiopian-Afar superplume, this zone dips to the south-west. Perhaps, it is a relic of a previously existing plume.

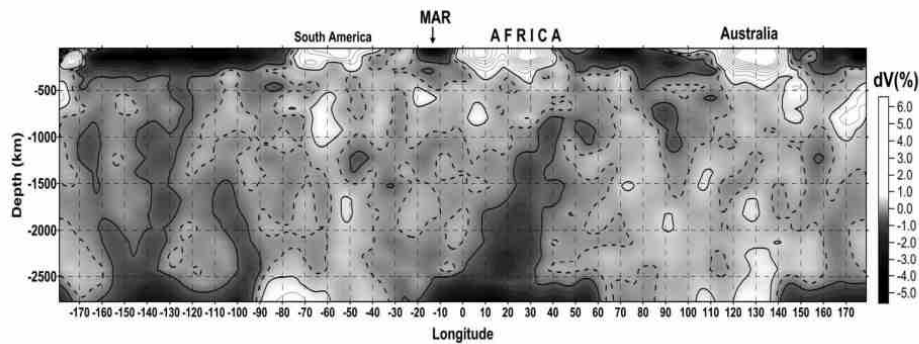


Fig. 30. Seismic tomography  $dV_p$  section along  $S22^\circ$  latitude. The "branches" of Pacific superplume are at the left part of section, the Ethiopian-Afar superplume is at the center of section. The both superplumes have continuation as lateral flows in upper mantle. Compiled after the data in (Becker, Boschi, 2002; Grand et al., 1997). Contour lines are spaced at 0.5%; the dashed line corresponds to zero value

We suppose that the elongated Ethiopian-Afar superplume developed as a more or less stationary structure at least from the end of the Paleozoic. The portions of moving Gondwana, which turned out to lie above the super-plume, underwent rifting that developed into spreading forming the Tethys Ocean. A flow of heated asthenosphere material from the superplume caused asymmetry of the spreading and moving of torn-off fragments of Gondwana to the north-east toward Eurasia. The oceanic Tethyan lithosphere subducted there and the Gondwanan fragments accreted to Eurasia. Because of this, the subduction zone jumped back to their rear (relative to Eurasia) parts. As a result, series of microplates, separated by sutures, accretionary wedges, and magmatic bodies related to different stages of the Tethys evolution, formed on the place of the future mountain belt. The recent structure of the mantle under the Indonesian segment, where the described process is lasting till now, give a possibility to suppose that the more north-western segments of the belt had previously the same structure, i.e., the subducted slabs transformed there at the depths of 400–700 km into the BMW that extended beneath the entire future mountain belt. The bulge of the upper high-velocity layer beneath the Southern Tibet (down to 400 km in the  $dV_S$  section) and the lower (~600 km) lens with slightly increased  $V_S$  may be the BMW relics. In the  $dV_p$  section, these lenses are separated by the low-velocity layer, which continues the sub-lithosphere flow related to the Ethiopian-Afar superplume.

The difference between the segments of the Alpine-Himalayan Belt is caused by their different Cenozoic history. The island-arc structure of the Indonesian segment has remained until now, whereas the last relics of the Neo-Tethys in the Pamir-

Himalayan segment were closed in the Oligocene. The relics of the Neo-Tethys and the related back-arc basins in the Arabian-Iranian segment were closed at the time from the Late Eocene to the Middle Miocene. In line with this, the subduction and the BMW formation gave way in the Pamir-Himalayan and Arabian-Iranian segments to the collision of the Eurasian and Gondwanan lithosphere plates. This process decelerated their convergence, but the hot asthenosphere flows from the Ethiopian-Afar super-plume probably prolonged the former movement and gradually spread under the entire orogenic belt. The propagation developed successively. For example, the sub-lithosphere low-velocity layer thinned sharply beneath the Greater Caucasus. The thinning could have been caused by subduction of the Para-Tethyan Caucasus basins under the Lesser Caucasus before the Middle Miocene (Leonov M.G., 1975; Alpine history..., 2007). The subduction hindered the northward propagation of the sub-lithosphere flow till the subduction had finished.

The hot sublithosphere flows reworked the upper mantle of the Alpine-Himalayan Belt. This is expressed in reduced average  $V_p$  values in the most upper mantle beneath all mountain systems of the belt, except a part of the Himalayan-Tibetan region (Fig. 25 & 29). The decrease of the velocities can be interpreted as a thinning of the lithosphere at the expense of the asthenosphere and/or decrease of density in the lithosphere mantle and the lower crust under the effect of the asthenosphere (Artyushkov, 1993; Ranalli et al., 2007; Trifonov et al., 2008; Trifonov, Sokolov, 2014; see sections 1.2.6 and 1.5.6). Beneath High Asia, where the lithosphere was essentially thickened by Cenozoic deformation, the high-velocity layer up to 300-km thick remained above the low- $V_p$  layer.

On moving, the sublithosphere flows were enriched in aqueous fluids that could derive from the former BMW lenses related to subduction zones. The asthenosphere, activated in this manner or its fluids penetrated into the lithosphere and gave rise to the important Cenozoic geological processes. The effect of the active asthenosphere and related fluids induced softening of the lithosphere (Artyushkov, 2003) that promoted intensive deformation, detachment, and large lateral displacement resulted in the formation of local uplands in the stage 1 of mountain building. Local uplands formed in the areas of concentrated deformation. Their position depended on orientation of maximum compression that was different in different substages of the stage 1. Formation of the local uplifts occurred against the background of neotectonic evolution of the lithosphere that developed according to two scenarios, the Central Asian and the Mediterranean.

In Central Asia, the lithosphere was thickened by previous significant deformation and contained a lot of metabasic relics of the former oceanic crust. The effect of the active asthenosphere and related fluids caused the metamorphic reworking of metabasic relics and the formation of intra-lithosphere magmatic sources, including crustal ones that were expressed by gigantic granitic batholiths (Letnikov, 2003<sub>1</sub>). These processes resulted in predominating rise of the territory that combined with the local deformational uplifts.

In the Mediterranean, the deformational uplift in the areas of maximum compression developed parallel to subsidence of secondary basins that formed after the closure of Neotethys and majority of its back-arc basins. Some secondary basins were deep enough for pelagic sedimentation. Such basins developed around the northern flank of the Arabian Plate in the Eocene and were deformed and closed in the Miocene (Robertson et al., 2004). In Western Mediterranean, similar structures (the Ligurian, Tyrrhenian, and possibly Alboran basins) have formed after the folding of late Middle Eocene and develop till now. Their origin can be related to the upper mantle diapirs that rise from the active asthenosphere through the relatively thin lithosphere of the region.

Large-scale deformation of the stage 1, accompanied by metamorphism and crustal magmatism caused a consolidation of the Earth's crust to the Early Pliocene. The consolidation was expressed by cessation of the large-scale granite formation in the Pliocene–Quaternary and localization of volcanic activity within strike-slip zones (Koronovsky, Demina, 1999; Karakhanian et al., 2002; Wang et al., 2007; Trifonov et al., 2011). The latter became the leading form of transverse shortening of the belt at the stage 2, whereas the fold-thrust deformation concentrated within the basins with thick sedimentary cover, such as the Sub-Himalayas, Afghan-Tajik Basin, foothills of the Taurus, the Lower Zagros, and periclinal of the Greater Caucasus.

Huge strike-slip fault system formed in the Alpine-Himalayan Belt during the stage 2 (Fig. 31). Some segments of these systems developed as strike-slip faults earlier, another ones appeared only in the Pliocene–Quaternary. The largest dextral system striking in the NW–SE to the W–E direction begins in the NW by the Talas-Fergana Fault. It continues to the SE en echelon by the Karakorum Fault Zone and the W–E-trending en echelon row of the South Tibetan strike-slip faults. Farther to the SE the system bifurcates to two strands. One of them is the Red River Fault that extends into Vietnam. The second strand extends to the south by the dextral strike-slip faults of the southern Yunnan and the northern Burma that continue en echelon by the dextral Sagaing Fault and probably by the faults of the off-shore East Indian

Ridge. The similar large system includes several right lateral fault zones: the North Aegean, North Anatolian, Main Recent Fault of Zagros, and its continuations in the Fars tectonic province of Iran. One more such system is represented by the reverse-dextral Main Copet Dagh Fault that continues en echelon to the west by the Isak-Cheleken, Apsheron Threshold and Main Great Caucasus fault zones.

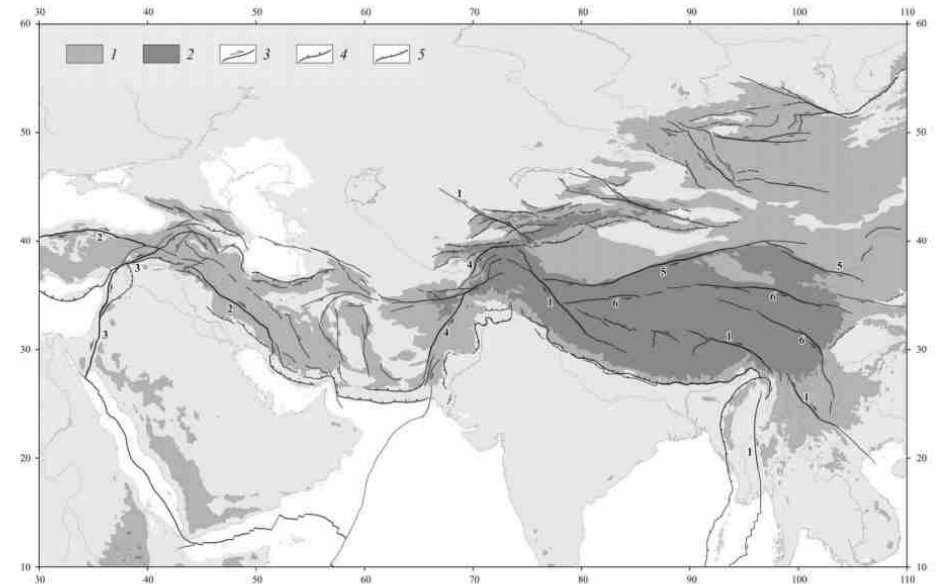


Fig. 31. The Pliocene-Quaternary strike-slip systems in the Alpine-Himalayan Belt

1, highlands 1000–3000 m; 2, ridges and plateau higher than 3000 m; 3–5, major active faults: 3, strike-slip faults, 4, thrusts and reverse faults, 5, normal faults. The largest dextral strike-slip systems: 1, the system from the Talas-Fergana Fault up to the Red River and Sagaing faults; 2, The North Anatolian fault zone and Main Recent Fault of Zagros with its continuation. The largest sinistral strike-slip systems: 3, Levant–East Anatolian; 4, Darvaz–Chaman with its southern off-shore continuation; 5, Altyn Tagh; and 6, Kunlun–Yunnan

There are also several large N–S-trending and SW–NE-trending sinistral fault systems. One of them is formed by the Dead Sea Transform (the Levant fault zone) and the East Anatolian fault zone that bifurcates in the NE to the North-East Anatolian and East Anatolian strands. They continue to the NE by the Kazbek-Tskhinval fault, possibly extending to Daghestan. Another dextral system includes the Darvaz and Chaman sinistral faults and the southern en echelon continuation of the latter that extends possibly to the south by the Owen fault zone in the off-shore Merrey Ridge of the western Indian Ocean. Two more sinistral systems are the ENE-trending Altyn Tagh and Kunlun–Yunnan fault zone in Central Asia.

Under the consolidated crust, the influence of the asthenosphere onto the lithosphere increased at the stage 2 of mountain building. According to the seismological and gravimetric data, a density of the uppermost mantle is decreased under the highest mountain systems of Central Asia (the Himalayas, the Tibet, the Kunlun, the Pamir–Hindu Hush–Karakoram region, and the Central and Eastern Tien Shan) as well as under the Lesser Caucasus and the Eastern Carpathians (see the section 1.5.5.3). The most probable mechanism of the decrease of density is partial replacing of the lithosphere mantle by the lower-dense asthenosphere (Artyushkov, 1993, 2003; Trifonov et al., 2008, 2012<sub>1</sub>). The decrease of density of the uppermost mantle leads to the uplift of the Earth's crust.

The decrease of density of the lower crustal masses as a result of retrograde metamorphism under the effect of cooled Pliocene asthenosphere fluids may be the second source of intensification of mountain growth. Influence of this factor seems to be dominant on the additional uplift of the Greater Caucasus above that due to the compression deformation. The decrease of density of the uppermost mantle is found only under the Elbrus volcanic region (Milanovsky et al., 1989). At the same time, volumes of rocks with the lowered density and increased electric conductivity were found under the Central and Eastern Caucasus in the lower crust and near the crust-mantle boundary (Grekov et al., 2008). Such volume under Elbrus at the depths of 35–50 km is characterized by the lower seismic wave velocities and is identified as a magmatic source (Modern and recent volcanism..., 2005). However, this interpretation cannot be applied to the other similar volumes. Decrease of their density is probably due to the retrograde metamorphism of rocks near the crust-mantle boundary with participation of the cooled asthenosphere fluids (Trifonov, Sokolov, 2014). Their main source was the asthenosphere flow from the Ethiopian-Afar superplume that reached the Greater Caucasus only in the Late Miocene (Ershov, Nikishin, 2004). Small thickness of the flow explains its weak expression in the field of seismic wave velocities. However, this thin flow and its fluid influence were able to facilitate the metamorphic decrease of density of the high-grade metamorphic rocks of the crustal origin that resulted in the uplift of mountain system. We suppose the same development of the Late Cenozoic tectonic processes in the Western Tien Shan (Trifonov et al., 2012<sub>2</sub>).

The both above-mentioned processes produced additional rise of the land surface and caused the acceleration of total uplift of the belt during the Pliocene-Quaternary.

## **2.2.2. Cenozoic volcanism in the Arabian Plate and Arabian-Caucasus Segment of the Alpine-Himalayan Belt**

An analysis of dates of the Cenozoic volcanic rocks in the East African rift system and the Arabian-Caucasus segment of the Alpine-Himalayan Belt give a possibility to estimate spread of the sublithosphere upper mantle flow away from the Ethiopian-Afar superplume (Fig. 32).

### **2.2.2.1. Basaltic volcanism in the Arabian Plate**

The East African rift volcanism began in the Eocene 45–37 Ma (Ebinger, Sleep, 1998). In the Oligocene, the Aden–Red Sea rift system was originated, and the belt of basaltic parallel dykes, small volcanoes and extrusions formed in the northeastern side of the Red Sea rift. According to the data on Saudi Arabia, volcanism started in the belt 32–30 Ma and continued till ~20 Ma with maximum 21–24 Ma (Camp, Roobol, 1992). In the Sinai part of the belt, dykes, sills and extrusions have the K-Ar ages from  $24,8 \pm 1,5$  Ma till  $20,3 \pm 0,7$  Ma [Segev, 2005]. During the Late Oligocene–Early Miocene, the basaltic volcanism occupied large areas in the central and northern parts of the Arabian Plate (Camp, Roobol, 1989). The basalts are in Syria (Geological Map of Syria, 1964; Ponikarov et al., 1967; Mouty et al., 1992; Chorowicz et al., 2004) and in adjacent territories of Turkey up to the Taurus suture (Çapan et al., 1987; Yilmaz et al., 1998) and in Jordan up to Saudi Arabia (Barberi et al., 1979; Ilani et al., 2001). Similar, but less extensive volcanism occurs in the Dead Sea Transform (DST) zone (Garfunkel, 1989; Sharkov et al., 1994; Polat et al., 1997; Yürür, Chorowicz, 1998; Abdel-Rahman, Nassar, 2004; Segev, 2005).

All researchers agree that the basalts were generated in the mantle, but attribute their origin to different processes. In the opinion of Garfunkel (1989), the basalts were related to “several short-lived upwellings, which formed intermittently beneath a wide region”. Stein and Hofmann (1992) came to the conclusion that relative homogeneity of the basalts in terms of the Sr–Nd isotopic ratios was due to their common source represented by a plume at the base of the Arabian lithosphere. Sobolev et al. (2005) agreed with the “plume” origin of the Arabian basalts, but argued they are related to the Ethiopian-Afar deep mantle superplume. Ershov and Nikishin (2004) shared this opinion. They reasoned that the superplume penetrated to the upper mantle from the lower mantle 45–37 Ma (Ebinger, Sleep, 1998) and formed two lateral sub-lithosphere flows: to the south (Kenya) and to the north.

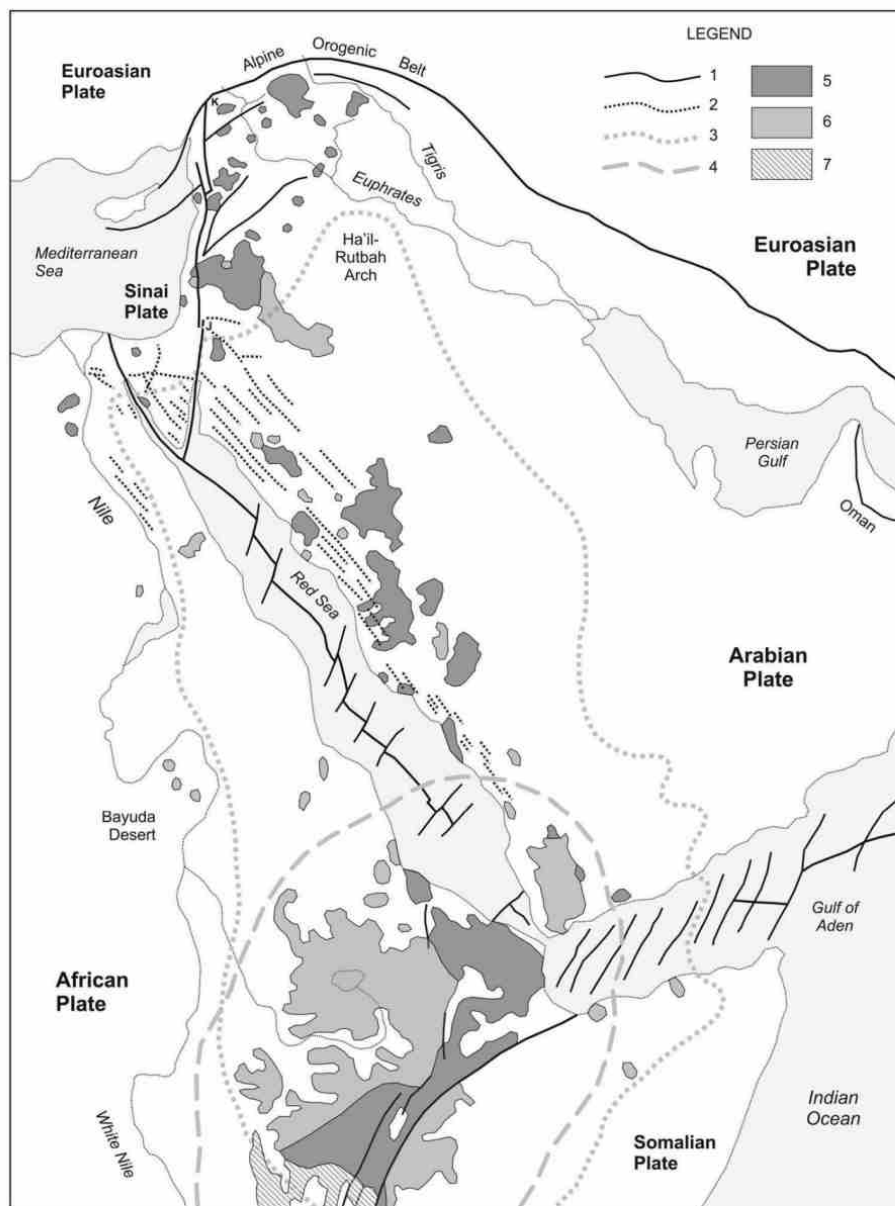


Fig. 32. The Ethiopia–Arabian plate volcanism, modified after (Segev, 2005). 1, main faults; 2, Middle Cenozoic dykes; 3, boundaries of the Afro-Arabian dome; 4, boundaries of the Ethiopia–Afar mantle plume; 5, Late Cenozoic volcanics; 6, Middle Cenozoic volcanics; 7, Early Cenozoic volcanics

The second flow propagated in succession beneath the southern Arabia and Red Sea region (~28–27 Ma), beneath central and northern Arabia (13–9 Ma), the Armenian Highland (~11 Ma) and the Greater Caucasus (9–7 Ma). Ershov and Nikishin referred to the seismic tomography data on existence of the “hot” (low-velocity) sublithosphere volumes beneath these regions (Debayle et al., 2001; Ershov et al., 2001) as an evidence of the flow.

However, Lustrino and Sharkov (2006) raised objections against links between the basalts and sublithosphere plumes: (1) “the spinel/garnet-bearing lherzolitic sources evidenced by semi-quantitative geochemical modeling can be related only to relatively shallow sources (generally <90 km deep)” (p. 136), i.e., in the lower lithosphere; (2) the absence of one-way progression of the magmatic activity age and the long time span of eruptions in the same areas do not correspond to the deep mantle plume volcanism; (3) the differences in Sr and Pb isotopic ratio exclude any participation of the Afar plume in generation of the central-northern Arabia basalts. Lustrino and Sharkov (2006) “propose that lithospheric extension is the main cause of igneous activity” and emphasize its “structural control by lithospheric discontinuities representing preferential pathways for uprising magmas” (p. 135). According to Weinstein’s data, quoted by Segev (2005), the Galilee–Dead Sea region basalts were lithosphere-derived and could have “two principal sources: amphibole-rich peridotite”, related to the Late Proterozoic slab and “amphibole-garnet-rich pyroxenitic veins within the peridotite source, produced by the Paleozoic within-lithosphere partial melting event”. Weinstein et al. (2006) linked the basalts with heat “from thermally anomalous zone within the sublithospheric mantle”.

Contradiction of views on the basalt origin is caused by the lack of the data on or attention to geological history of the volcanism and relationships between it and neotectonic evolution of the Arabian Plate. This impelled us to carry out the studies of geology and additional K-Ar dating of the Late Cenozoic basalts in Syria. We corrected distribution of Holocene basalts, carried out the K-Ar dating (21 new dates) and paleomagnetic studies of some lava flows, studied relationships of the flows with bedrock and capping layers (Trifonov et al., 2011; Neotectonics, recent geodynamics and seismic hazard assessment of Syria, 2012). The new ages of the basalts together with 71 earlier K-Ar and  $^{40}\text{Ar}$ - $^{39}\text{Ar}$  age determinations (Giannérini et al., 1988; Sharkov et al., 1994, 1998; Sharkov, 2000; Demir et al., 2007) give a possibility to correct the map of basalts (Fig. 33), to outline the history of the Late Cenozoic Syrian volcanism and to correlate it with tectonic structure and evolution. This gives a new view on origin of the basalts.

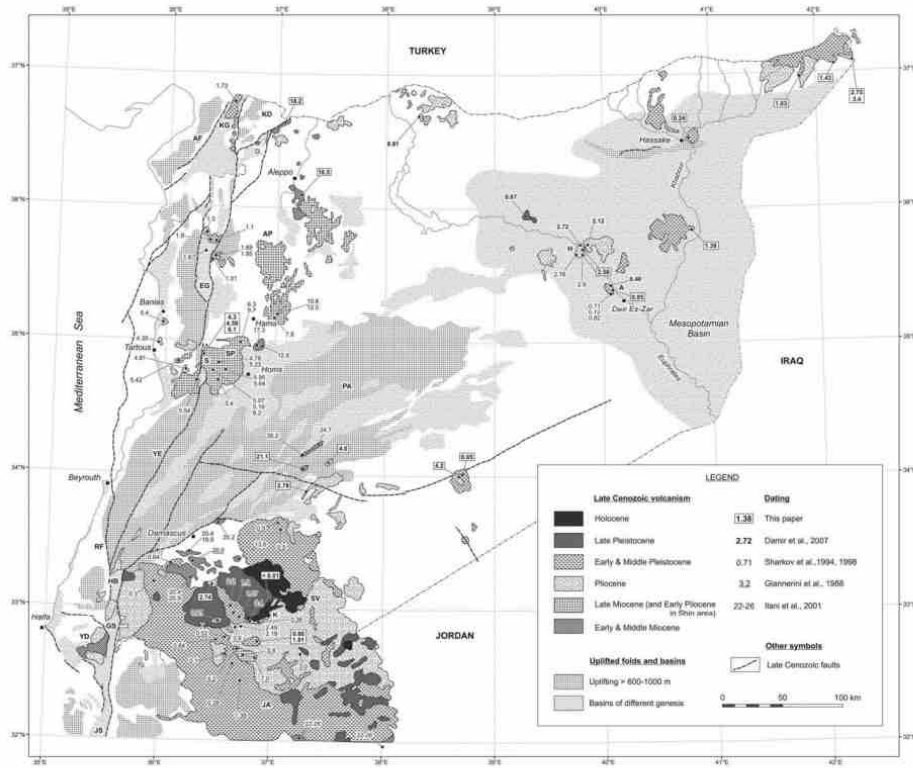


Fig. 33. Structural-geological map of Neogene-Quaternary basalts in Syria and adjacent territories (Trifonov et al., 2011). Structural features and basaltic fields: AF, Amanos fault (East Anatolian fault zone); AP, Aleppo Plateau; EG, El Ghab pull-apart basin, segment of the DST; GS, Galilee Sea pull-apart basin; HB, Hula pull-apart basin; JA, Jebel Arab (Harrat Ash Shaam) Highland; JS, Jordan Valley segment of the DST; KD, Kurd Dagh ridge; KG, Karasu graben; PA, Palmyrides; RF, Roum fault; SP, Shin Plateau; SV, Safa volcano; YD, Yizre'el depression; and YF, Yammuneh segment of the DST. Sites: A, Ayash village; H, Halabiyeh lava field; K, Kra lava field; and S, Saraya section

The Late Cenozoic basalts are represented in Syria and the adjacent territories by multi-age lava flows often overlapping each other. Less common are basaltic tephra and spatter in and near volcanoes, as well as pyroclasts and hyaloclasts. The latter have been recorded in the Dead Sea Transform (DST) grabens and near the Mediterranean coast. Dykes have been found in ruins of some volcanoes and in lava flows on both sides of the DST.

The Jebel Arab Highland is situated in southwestern Syria and continues to Jordan up to Saudi Arabia, where it is known as Harrat Ash Shaam. It is the largest Late Cenozoic basaltic field in the region, far exceeding other fields in height and extent.

One of the lesser fields is the Shin Plateau on the eastern side of the DST to the west of the city of Homs. Analogous basalts are known there on the western side of the young strand of the DST, some of them form a continuation of the Shin basalts, offset sinistrally to 16–20 km on that strand (Chorowicz et al., 2004). Until the beginning of the Pliocene, the most active strand of the DST was the Roum Fault and its continuation on the continental slope (Trifonov et al., 1991; Barazangi et al., 1993; Rukieh et al., 2005; Neotectonics, recent geodynamics and seismic hazard assessment of Syria, 2012). So, the basalts on both sides of the young DST strand were erupted on the Arabian Plate. Relatively small basaltic flows are known in the Palmyrides and in the northern part of the Syrian Desert. The basalts are more widely spread on the Aleppo Plateau near the cities of Hama and Aleppo and continue from there northwards up to the Turkish town of Kahraman-Maraş (Çapan et al., 1987). Lava fields formed by one or several flows are known in the Euphrates valley and in the northwestern part of the Mesopotamian Foredeep. Basalts of the northern margin of the Foredeep are continued with larger basaltic fields in the southeastern Turkey.

In the DST zone, the Late Cenozoic basalts are exposed in the northern part of the El Ghab pull-apart basin and in the Karasu graben between the northern termination of the DST and the Amanos Fault of the East Anatolian fault zone (EAFZ). Farther south, the basalts are exposed on the surface or are penetrated by bore holes in the Hula pull-apart basin and the Jordan valley; they cover vast areas in the Yizre'el depression near the Galilee Sea (Garfunkel, 1989; Hirsch, 2005; Segev, 2005). The latter areas represent the western termination of the Jebel Arab lava field, offset sinistrally on the DST (Segev, 2005). Near the Dead Sea, the basalts are exposed on the eastern side of the DST and appear along its western side only near the Red Sea as a part of the Dyke Belt.

The Late Cenozoic basalts were erupted by small volcanoes, ruins of which are found on the basaltic fields. Some eruption centers are so morphologically inexpressive that their location was identified only by relative elevation of different parts of the lava surface and by traces of lava flow, if the surface was preserved sufficiently well. In the Jebel Arab Highland, fissure eruptions predominate. Centers of eruption form the NW-trending and NNW-trending linear chains, which represent extensional faults. Some chains are formed by volcanoes of different age, for example, the Late Miocene and Pliocene or Pliocene and Pleistocene. That indicates a long duration and inheritance of the volcanic process, in contrast to basaltic volcanism in rift zones of Iceland as a part of the Mid-Atlantic Ridge. The Icelandic linear volcanic chains have been active for a short time (Trifonov, 1978). Linear

location (the NW–SE trend) is characteristic also of volcanoes in the Shin Plateau (Chorowicz et al., 2004). The N–S-trending groups of volcanoes are situated on the normal-sinistral faults or form short parallel chains in the northern part of the DST. Besides the fissure eruption zones, there are single small volcanoes and their nonlinear groups as well as rare shield volcanoes (such as the Safa Holocene center) in the Jebel Arab Highland.

Composition of the Late Cenozoic Syrian basalts is generally similar to that of basalts in the adjacent parts of the Arabian Plate (Alici et al., 2001; Shaw et al., 2003; Segev, 2005). The Syrian basalts are mostly alkaline mafic rocks with high (1.8–3.7 %) content of TiO<sub>2</sub> (basanites, hawaiites and alkali basalts) and more rarely transition/tholeiitic basalts with 44.3 to 52.5 % of SiO<sub>2</sub>. The Na<sub>2</sub>O/K<sub>2</sub>O ratios vary from ~1.5 to 5.6 and show positive correlation with the SiO<sub>2</sub> content (Sharkov et al., 1994; Sharkov, 2000; Lustrino, Sharkov, 2006). The <sup>87</sup>Sr/<sup>86</sup>Sr ratios (0.70321 to 0.70485) show negative correlation with the <sup>143</sup>Nd/<sup>144</sup>Nd ratios (0.512938 to 0.512842) (Lustrino, Sharkov, 2006). There are some peculiarities of basalt composition in different volcanic areas. The relatively high alkalinity is characteristic of basalts in the Shin Plateau and its coastal continuation; low alkalinity basalts predominate in the Jebel Arab Highland, while tholeiites are typical of the southern Aleppo area (Sharkov, 2000).

Lustrino and Sharkov (2006) divided the Syrian basalts into two groups: (1) with ages between ~25 and ~5 Ma and (2) younger than ~5 Ma. In each group, content of the incompatible trace elements increases with decrease of the age as a result of fractional crystallization in magmatic sources. An abrupt change in basalt composition occurred ~5 Ma ago. That was decrease in TiO<sub>2</sub>, Na<sub>2</sub>O, K<sub>2</sub>O, P<sub>2</sub>O<sub>5</sub> and incompatible trace elements, while neither MgO proportion decreased, nor that of SiO<sub>2</sub> increased. The authors above explain these phenomena by “increasing degree of partial melting and/or shallower depths of partial melting (i.e., increasing percentage of spinel in lherzolitic mantle)”. By Lustrino and Sharkov (2006), the ~5 Ma adiabatic melting could follow the upper mantle decompression caused in turn by some re-organization in plate motions (Barazangi et al., 1993; Zanchi et al., 2002; Rukieh et al., 2005). It is worth noting, however, that the conclusion of Lustrino and Sharkov (2006) about the ~5 Ma event is based only on the data from the Shin Plateau and its coastal continuation, so that the event could have rather local than regional geodynamic cause.

The Late Cenozoic pyroclasts and some basalts include mantle xenoliths mainly of the spinel lherzolites and the spinel and garnet-spinel websterites, and rare xenoliths

of pyroxene granulites, probably representing the old oceanic crust (Sharkov et al., 1996; Sharkov, 2000). The absence of xenoliths of the lower crust garnet granulites and of the upper crust material suggests that the intermediate magmatic sources were not characteristic of the Late Cenozoic volcanism.

There is some correlation between periodicity in volcanism activity and structural evolution of the plate boundaries. Four phases of neotectonic evolution in active zones surrounding the Arabian Plate, corresponding to the same phases in other parts of the Alpine-Himalayan Belt (see chapter 1.5) were identified. During the first, Late Oligocene–Early Miocene, substage, the Aden–Red Sea rift system was originated, and the belt of parallel dykes, small volcanoes and extrusions formed in the northeastern side of the Red Sea rift. The Arabian Plate moved to the NNW and produced sinistral slip on the DST and shortening in the northwestern margin of the plate. The NNW–SSE compression was accompanied by the ENE–WSW extension. That favored opening of extensional faults and volcanic activity, as most of magmatic channels marked by volcanic chains and interpreted as extensional faults strike NNW–SSE here. Two Late Oligocene dates (26.2±2.1 and 24.7±1.4 Ma) were obtained in the western part of the Ed Dau Basin in the Palmyrides, where the basalts occur near the bottom of the Upper Cenozoic fine-grained continental deposits. The Early Miocene basalts dated from 21.1±0.9 Ma to 17.3±0.8 Ma are more widespread (Fig. 33). In general, the Late Oligocene and Early Miocene sub-aerial volcanic area forms a relatively narrow N-trending band in the western part of the Arabian Plate approximately parallel to the DST (Trifonov et al., 2011). The band extends from the northern slope of the Jebel Arab Highland up to the Aleppo Plateau and the Kurd Dagh foothills and continues beyond the Syrian boundaries to the north and to the south. In the north, in Turkey, the K-Ar dates 18.6±0.8, 17.1±0.8 and 16.5±0.6 Ma (Arger et al., 2000), and 19.1±1.3 and 17.0±0.7 Ma (Tatar et al., 2004) were obtained in the large lava field to the SE of the town of Kahmaran-Maraş. In the south, in Jordan, the oldest basalts with the K-Ar ages of 26–22 Ma were found at the eastern margin of the Harrat Ash Shaam and in its central part, where the basalts compose ruins of older volcanoes (Ilani et al., 2001).

After the short episode of the rifting abatement, during the second, Middle Miocene, phase, the Arabian Plate moved to the NE. The NE–SW compression and the NW–SE extension did not favor volcanic activity in the N-trending band. Volcanism waned in Syria and ceased in the Jordanian part of Harrat Ash Shaam. The Middle Miocene basalts (17–13 Ma) were found only in the north of the Jebel Arab Highland and near the city of Homs. Decrease of volcanic activity was reported also

in Saudi Arabia, in the north-eastern side of the Red Sea rift (Camp, Roobol, 1992). This phase of the tectonic and volcanic quiescence began in the north later (~17 Ma) than in the south (~20 Ma), as seen in the distribution of dated basaltic flows (Fig. 34).

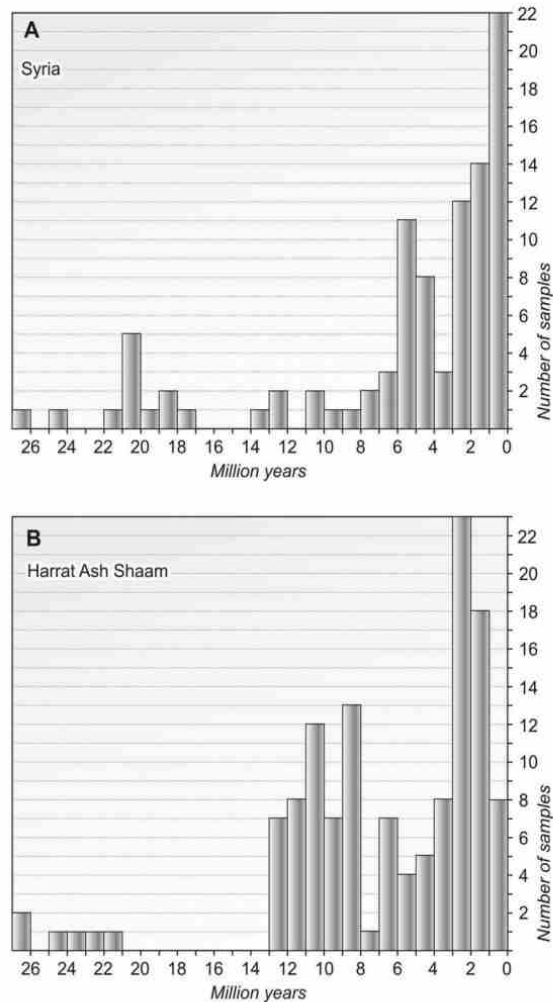


Fig. 34. Histogram of age distribution of the available K–Ar and Ar–Ar dates of the Syrian basalts, by the data in (Giannérini et al., 1988; Sharkov et al., 1994, 1998; Demir et al., 2007; Trifonov et al., 2011), in comparison with analogous histogram for the Jordanian part of the Harrat Ash Shaam (Ilani et al., 2001). N is number of the dates

At the third phase, in the Late Miocene and particularly in Messinian, the compression and shortening was directed again to the NNW that favored volcanism. Renewal of eruptions began ~12 Ma, though the volcanism was weak till the end of the Tortonian. The lava flows, dated at 12–7 Ma are confined to the same N-trending band, the latter in its northern segment expanded eastwards to the Euphrates and westwards onto the north-eastern part of the Shin Plateau. The date  $9.7 \pm 0.6$  Ma from the Shin Plateau marks beginning of its activity, which propagated later to the west.

The tectonic movements intensified in the Messinian. That caused folding and thrusting in the Palmyrides. At the same time, ~6.3 Ma, volcanism sharply intensified and continued in the Early Pliocene till ~4 Ma. It occupied not only the Jebel Arab Highland, but large areas in the Shin Plateau and its western continuation up to the

Mediterranean coast near the towns of Tartous and Banias. The geochemical features of the Shin basalts described above suggest either a higher degree of partial melting or its shallower depth, i.e. decompression in the mantle source (Lustrino, Sharkov, 2006). It is not inconceivable that the formation of the source of the Shin lavas was somehow related to shortening in the Palmyrides. A probable scenario implies that, together with sinistral motion on the DST, the shortening caused the NE-directed movement of the Aleppo Block and subsequent decompression in the southwestern part of the block, which resulted in the Shin volcanism. Changes in the lithosphere, associated with the magmatism caused drastic changes in the northern part of the DST. New strand of the DST formed in the Shin area. It became the main strand and propagated to the south (Yammunch segment) and to the north (El Ghab segment) up to junction with the newly formed EAFZ (Zanchi et al., 2002; Rukieh et al., 2005). The moment of restructuring of the DST system was manifested by brief wane of volcanism ~4–3.5 Ma.

The Late Miocene – Early Pliocene phase of volcanism was somewhat different in the Jordanian part of the Harrat Ash Shaam. Volcanism was resumed ~13 Ma there and continued (with brief hiatus at ~7 Ma) until 3 Ma, when the next reactivation of volcanism took place (Ilani et al., 2001). We estimate these changes by number of the basaltic dates of different ages (Fig. 34). Of course, they show only distribution of dated basaltic flows over the land surface and can not correspond exactly to epochs of rise and fall of volcanic activity, but general tendency is probably indicated by number of the dates.

The Yizre'el depression between the Galilee Sea – Lower Jordan valley and the Haifa fault zone occupies a particular position among volcanic areas of the region (Garfunkel, 1989). Five basaltic flows alternate with clastic deposits of the Herod Formation on the southwestern coast of the Galilee Sea near the village of Poriya (southwards of the town of Tiberias). Three lower flows are characterized by the  $^{40}\text{Ar}$ - $^{39}\text{Ar}$  dates from  $16.05 \pm 0.07$  to  $15.34 \pm 0.05$  Ma, and the upper flow is dated as  $13.31 \pm 0.06$  Ma (Segev, 2005). These flows are covered by several flows with the K–Ar dates 12.5–10 Ma. In addition,  $^{40}\text{Ar}$ - $^{39}\text{Ar}$  dates have been obtained eastwards of the village of Afula:  $14.9 \pm 0.1$  and  $13.9 \pm 0.1$  Ma [Segev, 2005]. The described rocks are united into the Lower Basalt Group with thickness up to 630–650 m to the south-west of the Galilee Sea and near the village of Afula (Segev, 2005). The dates of the Lower Group show that the volcanic activity continued through the Middle Miocene without any signs of attenuation typical of Syria and Jordan. The Late Miocene basalts with ages ~9 to 6–5.7 Ma form flows of small thickness in the Lower Galilee

and on the Golan Hills and represent an epoch of relative wane of volcanic activity. The next burst of eruptive activity produced the Cover Basalt (Bashan Group) 55–175 m thick dated by the  $^{40}\text{Ar}$ - $^{39}\text{Ar}$  from  $5.1\pm 1$  to  $3.5\pm 0.1$  Ma (Segev, 2005). So, a sequence of the Miocene–Early Pliocene volcanic events near the Galilee Sea and in the Yizre’el depression repeated the Syrian “scenario” with some delay. Voluminous eruptions occurred there  $\sim 16$ – $10$  Ma and in the interval between  $5.1\pm 0.1$  and  $3.5\pm 0.1$  Ma, with an epoch of low volcanic activity in-between (Segev, 2005). Perhaps, that depended on location of the depression in the area of the two major faults junction (Garfunkel, 1989), where the geodynamic changes were manifested somewhat differently from the Arabian Plate.

During the Pliocene–Quaternary stage, the Arabian Plate moved to the north and underwent shortening in its northern boundary. The N–S-trending compression and the W–E-trending extension favored eruptions on the NNW-trending and N-trending extensional faults in Central and Northern Arabia. After the brief wane of volcanism  $\sim 4$ – $3.5$  Ma corresponding to the moment of the DST system restructuring, the volcanic activity resumed, became more intensive in the Late Pliocene and continued through the Pleistocene and locally Holocene. This volcanism was well pronounced on the Jebel Arab Highland and its Jordanian continuation, and showed itself farther to the east, in the northern part of the Syrian Desert, the Euphrates valley and the northern margin of the Mesopotamian Foredeep near the Turkish-Syrian boundary. There is no evidence of one-way rejuvenation of eruptions. For example, the Late Pliocene and Early Pleistocene lavas erupted nearly at the same location in the northern margin of the Mesopotamian Foredeep between the upper reaches of the Nahr El Khabour and the Tigris valley. A lava flow near the town of Hassake was dated even to the Middle Pleistocene ( $0.24\pm 0.06$  Ma) and eruptions could continue there in the Late Pleistocene. The same situation is characteristic for the Euphrates valley. In the DST, the eruptions began in the Early Pleistocene. Volcanoes were located on the N-trending boundary and inner faults of the Karasu valley ( $\sim 2$ – $0.4$  Ma) (Yürür, Chorowitz, 1998), in the El Ghab pull-apart basin (from  $1.9\pm 0.1$  until  $1.1\pm 0.2$  Ma) (Sharkov et al., 1994; Sharkov, 2000), the Hula pull-apart basin and the Jordan valley (from  $2.16\pm 0.28$  until  $0.95\pm 0.03$  Ma, according to the  $^{40}\text{Ar}$ - $^{39}\text{Ar}$  dating) (Segev, 2005).

The correlation between the main phases of evolution of the basaltic volcanism and neotectonics demonstrates genetic links between these processes in the Arabian Plate and its boundary zones and has to be taken into account for better understanding of the volcanism origin.

#### 2.2.2.2. Correlation of the Cenozoic volcanism in the Arabian Plate and in the Arabian-Caucasus segment of the Alpine-Himalayan Belt

A model of origin of the Late Cenozoic basaltic volcanism in Syria and the adjacent parts of the Arabian Plate must account for the following specific features of that volcanism.

1. Principal geochemical similarity of the basalts suggestive of mantle sources for the basalts (Stein, Hofmann, 1992).

2. Volcanic areas are characterized by inherited development. The largest of them evolved for a long time, 26 million years in Jebel Arab – Harrat Ash Shaam and more than 15 million years in the Aleppo Plateau. Moreover, even some of individual volcanic chains (e.g., in Jebel Arab) developed as inherited structures for several million years. There are no signs of one-way migration of the volcanism. Such a persistence of the volcanic areas means that the magmatic sources moved together with the Arabian Plate, i.e., magmatic sources were situated within the lithosphere mantle. This geological conclusion complies well with the results of geochemical studies of Weinstein (Segev, 2005) and Lustrino and Sharkov (2006).

3. Although only a part of volcanoes and basaltic fields demonstrate direct links with individual crustal structures of the Arabian Plate and its surroundings, there is a chronological coincidence between variations of volcanism intensity and its spatial distribution on one hand and geodynamic changes and tectonic events along the Arabian Plate boundaries on the other (Trifonov et al., 2011). In the favorable geodynamic situation the volcanism was renewed in the former zones or expanded into new areas. In the Shin area, geodynamically-controlled decompression of the lithosphere caused changes in chemical composition of basalts and essential changes in structure of the northern DST zone.

We propose the following explanation of origin of the Syrian Cenozoic basalts that may account for all the distinctive features mentioned above. A portion of the northern drift of the Arabian lithosphere plate is caused by motion of the plate on the asthenosphere flow. The flow moved away from the Ethiopia–Afar superplume, which rose from the lower mantle (Ebinger, Sleep, 1998; Ershov, Nikishin, 2004). The flow eroded the Arabian Plate deep interface, and magmatic sources were formed within decompressed sites of the lower lithosphere. As the potential of the sources was supported by the sublithosphere lateral flow, the sources could produce basaltic eruptions at the same areas for a long time. At the same time, eruptions were only possible, when the geodynamic setting favored initiation and activity of channels for

magma passage. Dependence of volcanism on the geodynamic situation explains synchronism in the occurrence of volcanic activity and tectonic events within and near the Arabian Plate. The local geodynamic changes in the Shin area led not only to the structural changes in the northern DST zone, but even caused temporal geochemical changes in the composition of the erupted basalts.

The composition of material involved in the sub-lithosphere flow changed in process of northward movement due to partial crystallization and inclusions of the asthenosphere material. The magma chambers in the lower lithosphere also included some local melted material. That is why geochemical traces of the Ethiopia–Afar superplume have been reliably established only in volcanic rocks in the southern part of the Arabian Plate (Altherr et al., 1990; Baker et al., 1997; Bertrand et al., 2003). Farther north, as in Syria, basalts lack the superplume characteristics (Lustrino, Sharkov, 2006).

The Arabian–Caucasus segment of the Alpine-Himalayan belt latter bears numerous manifestations of the Early Cenozoic volcanism. They are situated mainly near the former back-arc basins of the Neotethys and are probably related to their closing. The Oligocene was noted for attenuation of volcanism and formation of small granitic and granodioritic intrusions. Manifestations of the Early and Middle Miocene volcanism are very rare (Milanovsky, Koronovsky, 1973). Intensive volcanism began in the Late Miocene and continued until the Early Pleistocene and its weaker manifestations continued through the Middle and Late Pleistocene and locally occurred even in the Holocene. The volcanism occupied the inner zones of the orogenic belt from Central Anatolia up to Alborz and was most intensive on the Armenian Highland (Fig. 35). It spread to the central part of the Greater Caucasus as early as the Late Miocene and formed the subvolcanic extrusions in the area of Caucasus Mineral Waters. But maximum activity in the Elbrus and Kazbek volcanic areas is dated to the Late Pliocene – Early Pleistocene (2.8–1.5 Ma) (Koronovsky, Demina, 2007). Evidence of the historical eruptions was found in the Armenian Highland (the Syunik and Porak groups of volcanoes near the Khanarassar strike-slip fault in the Ghegam–Vardenis Upland, Ararat, and Tendurek and Nemrout volcanoes in the Van region) as well as in Central Anatolia (Ergiyas Dag and Hasan Dag), the northern Iran (Demaverd) and the Greater Caucasus (Elbrus) (Milanovsky, Koronovsky, 1973; Karakhanian et al., 1997, 2002; Bogatikov et al., 1998; Modern and recent volcanism..., 2005; Trifonov, Karakhanian, 2008).

Thus, the sublithosphere flow penetrated northward into the Arabian–Iranian segment of the Alpine-Himalayan belt only as early as the subduction of Tethys relics

at the southern margin of the belt completed in the Early Miocene (Robertson, 2000; Ershov, Nikishin, 2004; Robertson et al., 2004). The intensive volcanism, which rapidly spread from the Armenian Highland and Central Anatolia to Mount Elbrus, started in the Late Miocene. These volcanic manifestations are represented by wide spectrum of rocks from basalts up to ultra acid rocks. As a whole, the total composition evolved from andesite-dacites to andesites and basalts. They belong to the calc-alkaline series, although an increased alkalinity is reported in periphery of the volcanic areal (the Caucasus Mineral Waters, Kazbek, the north-east of the Armenian Highland, and the Demaverd volcano) (Koronovsky, Demina, 1999, 2007; Imamverdiev, 2000).

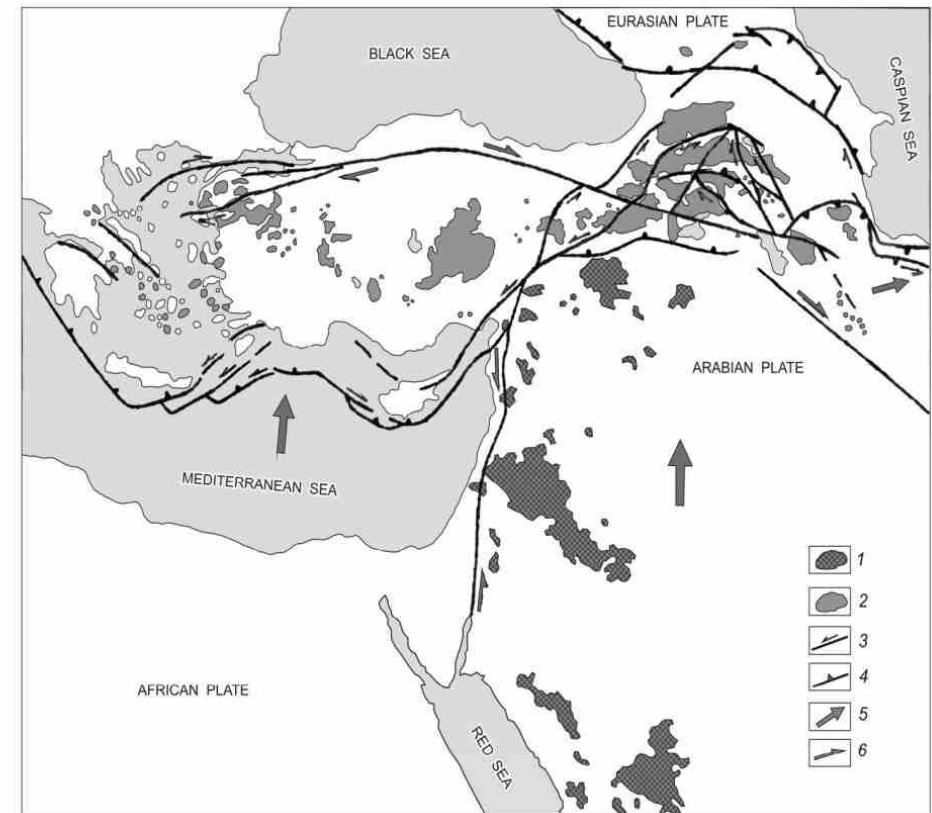


Fig. 35. The Oligocene-Quaternary volcanic formations and main faults of the Arabian-Caucasus region, modified after (Trifonov, Karakhanian, 2008)

1, Oligocene-Quaternary basalts of the Arabian Plate; 2, Neogene-Quaternary volcanic rocks of the Alpine-Himalayan Belt; 3, strike-slip faults; 4, thrusts and subduction zones; 5, direction of motion of plates and blocks; 6, direction of strike slip

Thermo-dynamic calculations based on the results of geochemical and petrological studies showed that magmas in the south of the Armenian Highland were generated under the pressure  $P=1.1\text{--}1.2$  Gpa characteristic for the upper mantle, while in the north of the Highland and in the Greater Caucasus, the level of the magma generation is characterized by  $P=0.95\text{--}1.05$  Gpa and  $T=850\text{--}1100^\circ$  that corresponds to the depths of 35–40 km, i.e. the bottom of the Earth's crust in the Highland and the lower crust in the Greater Caucasus (Koronovsky, Demina, 1999, 2007). In the Elbrus area, a depth of the acid magma generation is characterized by  $P=0.5\text{--}0.7$  Gpa, corresponding to the depths of 17–25 km. At a depth of 35 to 50 km beneath Elbrus there have been found a rock body with decreased velocities of seismic waves and increased electrical conductivity that may be identified with the magmatic source (Modern and Recent Volcanism..., 2005). So, the sources of the Late Cenozoic volcanism of the region were situated mainly in the lower crust and near the crust–mantle boundary.

Data of the Sr–Nd–O isotopic analysis of the volcanic rocks in the region, as well as high  $^3\text{He}/^4\text{He}$  ratios in water springs of Elbrus and Kazbek strongly suggest the mantle material to have penetrated to the magmatic sources (Ivanov et al., 1993; Bubnov et al., 1995; Polyak et al., 1998). Karyakin (1989) noted a similarity between the Armenian Highland basalts and basalts from ensialic island arcs and active continental margins. The decrease of the seismic wave velocities by 1.5% was found in the uppermost mantle beneath the Elbrus area (Milanovsky et al., 1989). Based on these data, Koronovsky and Demina (1996, 2004, 2007) proposed a model of the Late Cenozoic magma generation in the region. According to the model, the magma sources in the lower crust and the uppermost mantle formed under influence of heat and oxidation of fluids, transported from the deeper levels in the mantle. One of sources of the fluids could be deformational heating of the Mesotethys suboceanic slabs persisting within the lithosphere. At the same time, we agree with the idea of Ershov and Nikishin (2004) that the sublithosphere flow from the Ethiopia–Afar superplume could be another, and essential, source of the magma generation. The flow penetrated beneath the inner zones of the Alpine–Himalayan collision belt in the Miocene and reached the Greater Caucasus to the Upper Miocene. The Armenian Highland was subjected to both sources of the magma generation, which may account for the most intensive volcanism in the region (Trifonov et al., 2011).

### 2.2.3. Intracontinental mantle seismic-focal zones in the Alpine-Himalayan Belt

To contradict the study, we summarized catalog data (Kárník, 1968; Kondorskaya, Shebalin, 1982; Kondorskaya, Ulomov, 1995; Moïnfar et al., 1994; National..., 2007; Papazachos, Papazachou, 1997; Trifonov, Karakhanian, 2004) on the earthquakes, which took place in 1850–2007 and had  $M_S \geq 5$  and hypocenters at depths of  $\geq 40$  km ( $\geq 50$  km in thick-crust areas). Almost all such earthquakes are concentrated in the Hellenic and Cyprus arcs, Aegean region, Zagros Mountains, Vrancea megafocus, Middle Caspian, and Pamir–Hindu Kush zone with the Hindu Kush megafocus. The earthquakes in the Hellenic and Cyprus arcs are related to recent subduction zones. The other areas do not show such a relationship. The most active ones are Hindu Kush and Vrancea.

#### 2.2.3.1. The Pamir–Hindu Kush mantle seismic zone

Analyzing the catalog of strong ( $M_S \geq 5.7$ ) earthquakes in the central Alpine–Himalayan belt (Trifonov, Karakhanian, 2004), one may point out a small (100 x 150 km) area in northeastern Afghanistan with coordinates of 36–37°N and 69–71.5°E that is characterized by an anomalously great amount of released seismic energy (Fig. 12). About 20% of the energy released in the 20th century from all the earthquakes in the Alpine–Himalayan belt extending from the Dinarides to the Himalayas and Central Asia fell on this area. The overwhelming majority of earthquake hypocenters in this Hindu Kush seismic megacluster are concentrated in the upper mantle at depths of  $110 \pm 20$  and 190–240 (down to 270–300) km. East of the N-S-trending bend of the Pyandzh River (Fig. 11), the epicenters of strong mantle earthquakes are shifted farther to the north (up to 38°N) and are traceable as isolated clusters up to the southeastern termination of the Afghan-Tajik Basin. There, together with the Hindu Kush megacluster, they form the Pamir–Hindu Kush seismic focal zone. In the Pamirs, strong earthquakes are rare, their released energy is hundreds of times less than in the Hindu Kush, and their sources are concentrated at a depth of  $110 \pm 20$  km.

Geophysical characteristic of the zone. According to the seismological data, including low-magnitude events, the Pamir–Hindu Kush focal zone of intermediate earthquakes is a steep lens with variable thickness and changing density of hypocenters (Lukk, Nersesov, 1970). In both the Hindu Kush and Pamir segments of the zone, strong earthquakes occur at depths of  $110 \pm 20$  km (Fig. 36). Deeper, at